SCIENCE CHINA
Earth Sciences

•RESEARCH PAPER•

May 2021 Vol.64 No.5: 753–772
https://doi.org/10.1007/s11430-020-9752-6

Super-enrichment of lithium and niobium in the upper Permian Heshan Formation in Pingguo, Guangxi, China

Kunyue LING[1], Hanjie WEN[1,2,3*], Qizuan ZHANG[4], Chongguang LUO[1], Hannian GU[1], Shengjiang DU[5] & Wenxiu YU[6]

[1] *State Key Laboratory of Ore Deposit Geochemistry, Institute of Geochemistry, Chinese Academy of Sciences, Guiyang 550081, China;*
[2] *College of Earth and Planetary Sciences, University of Chinese Academy of Sciences, Beijing 100049, China;*
[3] *College of Earth Science and Resources, Chang'an University, Xi'an 710054, China;*
[4] *Guangxi Bureau of Geology & Mineral Prospecting & Exploitation, Nanning 530023, China;*
[5] *State Key Laboratory of Nuclear Resources and Environment, East China University of Technology, Nanchang 330013, China;*
[6] *Faculty of Land Resource Engineering, Kunming University of Science and Technology, Kunming 650093, China*

Received June 6, 2020; revised February 5, 2021; accepted March 2, 2021; published online March 17, 2021

Abstract The upper Permian Heshan Formation in Pingguo, Guangxi, China, is strongly enriched in lithium (Li) and niobium (Nb). The lower bauxite layer contains 0.02–0.04 wt.% Nb_2O_5 (averaging 0.035 wt.%), and the overlying clay rock layer contains 0.06–1.05 wt.% Li_2O (averaging 0.44 wt.%), both of which exceed the cut-off grades for independent Li and Nb deposits and are therefore highly prospective. In this study, a preliminary discussion of the genesis of the Li and Nb enrichment is presented to serve as a reference for the investigation, evaluation, and prospecting for clay- and sedimentary-type Li and Nb ores in other regions. The preliminary conclusions are that: (1) The bauxite ore contains abundant anatase, which positively correlates with the whole-rock concentrations of TiO_2 and Nb, indicating that the Nb is hosted mainly in the anatase; (2) the cookeite content in the clay rock positively correlates with the whole-rock Li concentration, indicating that cookeite is the main carrier mineral of Li, and its genesis can be attributed to reactions between clay minerals (e.g., pyrophyllite and illite) and Li-Mg-rich underground brine or pore water and groundwater in coastal areas; and (3) provenance analysis of immobile elements (Al, Ti, Nb, Ta, Zr, Hf, and rare earth elements) suggests distinct sources for the Nb-rich bauxite and the overlying Li-rich clay rocks, with the bauxite and Nb originating largely from alkaline felsic rocks in the Emeishan Large Igneous Province, and the clay rocks being derived from peraluminous or moderately fractionated felsic rocks associated with Permian Paleo-Tethyan magmatic arcs.

Keywords Heshan Formation, Critical metal, Lithium, Niobium, Super-enrichment

Citation: Ling K, Wen H, Zhang Q, Luo C, Gu H, Du S, Yu W. 2021. Super-enrichment of lithium and niobium in the upper Permian Heshan Formation in Pingguo, Guangxi, China. Science China Earth Sciences, 64(5): 753–772, https://doi.org/10.1007/s11430-020-9752-6

1. Introduction

Lithium (Li) and Niobium (Nb) are critical metals for modern energy and high-tech industries (Nico et al., 2016; Chen, 2019; Mao et al., 2019); their ores are usually found in granite and pegmatite, but are rare in sedimentary rocks (Zhu et al., 2001; Wang et al., 2013). In recent years, super-enrichment of Nb, zirconium (Zr), and rare earth elements (REEs) have been reported from the upper Permian Xuanwei and Longtan Formations in the eastern Yunnan, southern Sichuan, and western Guizhou regions of China, where they are thought to be derived from the Emeishan Large Igneous Province (ELIP) basalts or felsic rocks (He et al., 2007; Dai et al., 2010; Zhao et al., 2016; Du et al., 2019). Since the 1970s, several Li-rich rocks have been discovered in China's karstic (sedimentary) bauxite ore-bearing rocks in Guizhou,

* Corresponding author (email: wenhanjie@vip.gyig.ac.cn)

Henan, Shanxi, Yunnan, Guangxi, and Chongqing (Li et al., 2012; Liu et al., 2013; Wang et al., 2013; Zhao et al., 2015; Yang et al., 2019; Ling et al., 2018, 2020). Findings from these studies show that some sedimentary rocks are rich in Li and Nb and have potential as independent or associated mineral resources.

Recently, super-enrichment of Li was discovered in clay rocks and bauxitic clay of the Lower Carboniferous Jiujialu Formation in central Guizhou and the lower Permian Daoshitou Formation in central Yunnan (Wen et al., 2020). Analyses of more than 1000 samples show that the highest Li_2O content is >1.1%, with an average value of 0.3% (1400 ppm, 1 ppm=1 μg/g) (Wen et al., 2020). As Li is mainly hosted by clay minerals, and its formation is closely related to the carbonate basement, this Li deposit is defined as carbonate-hosted clay-type and constitutes a new Li resource (Wen et al., 2020). Based on the metallogenic model for carbonate-hosted clay-type Li deposit, an investigation and evaluation of Li resources in the karstic bauxite deposit region in western Guangxi resulted in the discovery of Li (maximum Li_2O content of 1.05%) and Nb (maximum Nb_2O_5 content of 0.04%) in the upper Permian Heshan Formation in Pingguo. This is an important breakthrough in prospecting for Li resource. In this study, a preliminary discussion of the mode of occurrence and enrichment mechanisms of Li and Nb is presented to serve as a reference for the investigation and evaluation of sedimentary-type Li and Nb resources in other regions.

2. Geological background

The Youjiang Basin (also known as the Nanpanjiang Basin) is located in western Guangxi in the southwestern region of the Yangtze Plate, between to the Song Ma suture zone in the south and the Permian (263–251 Ma) ELIP in the northwest (Figure 1a; Wu et al., 1999; Xu et al., 2001; Fan et al., 2004; Zhang et al., 2006; Cai and Zhang, 2009; Shellnutt, 2014). During the Early Paleozoic, the Yangtze Plate and the Indochina Block separated from Gondwana, drifted northward, and were subducted, forming the Permian (277–252 Ma) island arc igneous rocks, such as those found in the Truong Son belt. At the end of the Triassic, the plates amalgamated to form a single block, connected by the Song Ma suture zone (Metcalfe, 2006; Halpin et al., 2016; Ke et al., 2018; Xu et al., 2020).

At the end of the middle Permian, the Dongwu movement led to domal uplift in the upper Yangtze region and caused large-scale marine regression in southern China (He et al., 2003a; Sun et al., 2010). Uplift lasted ~3 Myr, during which the central area rose by several kilometres and western Guangxi by more than 100 m; this led to weathering and denudation of the middle Permian Maokou Formation limestone in western Guangxi to form the paleokarst landform (He et al., 2003a, 2010). At the same time, during the middle-late Permian (around the Guadalupian-Lopingian Boundary), massive volcanic eruptions occurred in the ELIP, covering an area of more than 250000 km^2. These were primarily basaltic and pyroclastic during the early stage, before felsic volcanic rocks such as trachyte and rhyolite were formed during the late stage, distributed over an area of ~10000 km^2 (Shellnutt, 2014; Yang et al., 2015). The greenhouse effect and acid rain caused by the ELIP eruptions increased continental weathering. Under the influence of strong weathering and denudation, the ELIP volcanic rocks developed weathering crusts, which were transported to and deposited in nearby basins (e.g., the Youjiang Basin) to form the Wuchiapingian clastic mainly including Xuanwei, Longtan, Wuchiaping, and Heshan Formation. The inner-intermediate zone of the ELIP volcanic rocks was not eroded entirely because of its considerable thickness (maximum of >5000 m), thus the Xuanwei Formation directly overlies the Emeishan basalts. The intermediate-outer zone of the ELIP volcanic rocks was completely eroded in some areas, in which the Longtan and Wuchiaping Formations were deposited upon the Emeishan Formation igneous rocks or unconformably on Carboniferous-Permian limestone. The outer zone of the ELIP volcanic rocks in western Guangxi was relatively thin (300–500 m) and was completely eroded, resulting in the Heshan Formation unconformably overlying the Maokou Formation limestone. The ELIP volcanic rocks and/or the Maokou Formation limestone provided stable sources for the development of Heshan Formation bauxites in western Guangxi area (Figure 1c; He et al., 2003a, 2010; Fan et al., 2008; Liu et al., 2017; Yu et al., 2019).

By the Permian, the Youjiang Basin comprised carbonate platforms alternating with inter-platform troughs. The troughs contained deep-water clastic deposits, and the platforms were dominated by shallow-water clastic and carbonate deposits (Figure 1a). These platform deposits, which constitute the middle Permian Maokou Formation, consist primarily of thick bioclastic carbonate and calcarenite. Unconformably overlying the Maokou Formation, the upper Permian Heshan Formation consists of a lower section of clastic rocks (generally bauxite and coal seams), and an upper section of limestone (Figure 1b; Yu et al., 2016). The clastic rocks is subdivided into a lower layer (~8 m thick) of purple, grey, or black bauxite, and pisolitic and oolitic bauxites, often with hematite or iron-rich bauxites, and an overlying clay rock layer (~10 m thick) of black carbonaceous clay rocks or coal seams, with minor grey and white clay rocks and silty clay rocks (Figure 1b; Yu et al., 2016).

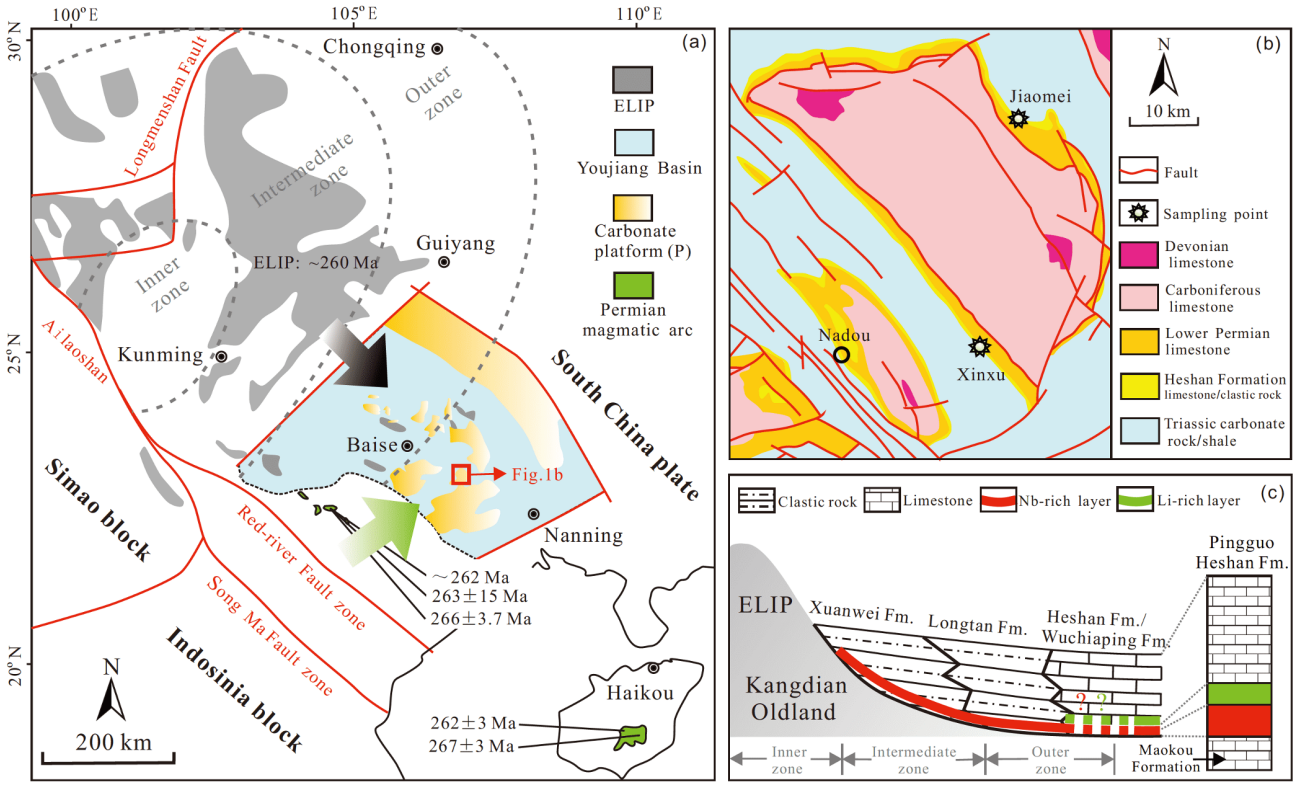

Figure 1 (a) Generalized tectonic domains of the southwestern Yangtze Plate and the middle-late Permian paleogeography of the Youjiang Basin (modified from Yu et al., 2016). The ages of the ELIP rocks are from Shellnutt (2014), and the ages of the Permian arc-related rocks are from Li et al. (2006) and Halpin et al. (2016). (b) Geological features of the Pingguo region, Guangxi (modified from Guangxi Bureau of Geology and Mineral Exploration and Development, 1985). (c) Paleogeographic map after the main phase of the ELIP activity, showing the location of the Li-Nb-rich Heshan Formation (modified from Zhao et al., 2016).

3. Sampling and analytical methods

Samples of the bauxite and clay rock layers of the lower part of the Heshan Formation were collected from complete sections in Jiaomei village (JM) in Jiucheng town and Xinxu village (XX) in Taiping town, Pingguo County, Guangxi. In addition, three samples of Maokou Formation limestone (XX-01, XX-02, and XX-03) were collected from the Xinxu section. Samples were collected and numbered sequentially in ascending stratigraphic order (Figure 1b). Representative samples were selected to make polished thin sections for scanning electron microscopy-energy dispersive spectroscopy (SEM-EDS). Analysis of the whole-rock mineral phase was performed using a Panalytical Empyrean X-ray powder crystal diffractometer (XRD) equipped with a PIXcel3D detector. The analytical method and conditions were as follows: Cu Kα target, 40 kV, 40 mA, and auto-flushing method for quantitative assessment of mineral contents. JADE software was used to compare the main diffraction peaks (d value and intensity) with standard cards to determine the main mineral phase composition, based on the best match. The semi-quantitative calculation used the formula $W_A=(I_A/R_A)/(I_A/R_A+I_B/R_B+I_C/R_C+\ldots)\times100\%$, where W_A is the weight percentage of the mineral phase, I_A is the strongest peak, and R_A is the reference intensity ratio (RIR) of the mineral phase to be measured (Table 1). The whole-rock trace elements and REE abundances were analysed through solution inductively coupled plasma-mass spectrometry (ICP-MS) analysis. The analysis was performed using a PlasmaQuant MS Elite ICP-MS, using the international standards OU-6, AMH-1, and GBPG-1 for quality control. Details of the method are described by Franzini et al. (1972) and Qi et al., (2000). The results have a relative standard deviation (RSD) better than 10% (Table 2). The analyses noted above were carried out at the Institute of Geochemistry, Chinese Academy of Sciences. In addition, analysis of major elements was performed by ALS Minerals-Guangzhou (China) and the analytical method were as follows: 200-mesh powder samples were melted using lithium metaborate or lithium borate, cooled, and then analysed by X-ray fluorescence spectroscopy (Table 2).

4. Results

4.1 Mineralogical features

The SEM-EDS and XRD analyses show that the bauxites are composed of diaspore, anatase, and illite, with small amounts

Table 1 The mineral abundance (XRD; wt.%) of bauxites and clay rocks from Pingguo area, Guangxi

Sample No.	Lithology	Thickness (m)	Diaspore	Kaolinite	Montmorillonite	Illite	Cookeite	Anatase	Quartz	Pyrite	Stilpnomelane	Dickite	Pyrophyllite	Gibbsite	Goethite
JM-01	Clastic bauxite	0.2	72.5			22		5.44							
JM-02	Clastic bauxite	0.4	71.2		1.1	21.8		6.07							
JM-03	Clastic bauxite	0.6	64.9			30.1		4.95							
JM-04-2	Clastic bauxite	0.8	72			18.9		3.92		5.2					
JM-05	Pisolitic bauxite	1	68.5			17.3		4.38		2.21	7.64				
JM-06	Clastic bauxite	1.2	68.4			19		5.59		1.71	5.3				
JM-07	Carbonaceous clay rock	1.4	7.26				16.8	1.38				6.86	67.7		
JM-08	Carbonaceous clay rock	1.6	10.3				12.3	2.47				4.17	65.8	4.09	
JM-08-2	Carbonaceous clay rock	1.8	1.04				6.42	2.49				5.79	80.7	3.51	
JM-08-3	Carbonaceous clay rock	2	11.2				11.6	0.82				5.55	66.4	4.27	
JM-09	Carbonaceous clay rock	2.2	8.11			3.11	25.4	1.49				8.51	47.8	5.52	
JM-10	Carbonaceous clay rock	2.4	10			2.35	8.13	0.9		1.12		5.91	66	5.65	
JM-11	Carbonaceous clay rock	2.6	7.26	1.33		41.3	40.1						9.94		
JM-12	Carbonaceous clay rock	2.8	6.57	1.17		46.5	37.4						8.35		
JM-13	Carbonaceous clay rock	3	3.41	0.73		41.1	32.4						22.4		
JM-14	Carbonaceous clay rock	3.2	6.09	0.53		35.5	35						24.5		
JM-15	Carbonaceous clay rock	3.4	6.71	0.59		47.2	38.5						6.96		
XX-04	Iron-rich bauxite	0.2	75.1		4.55			4.33							16
XX-05	Iron-rich bauxite	0.5	93.5					4.6							1.9
XX-06	Pisolitic bauxite	0.8	96					3.94							
XX-07	Clastic bauxite	1.1	94.4	1.51				4.06							
XX-08	Pisolitic bauxite	1.4	94.1	1.2				4.11	0.64						
XX-09	Pisolitic bauxite	1.7	95.4					4.61							
XX-10	Pisolitic bauxite	2	96					3.98							
XX-11	Clastic bauxite	2.3	93.8	2.2				4.02							
XX-12	Carbonaceous clay rock	2.6	23.6	21			6.2	1.65		29.8					17.8
XX-13	Carbonaceous clay rock	2.9	29.7	63				3.01	4.27						
XX-14	Carbonaceous clay rock	3.2	3.57	94.8				1.58							
XX-15	Carbonaceous clay rock	3.5	1.3	64.2		18.8	9.34	0.86							5.43
XX-16	Carbonaceous clay rock	3.8	22.7	77.3											

Table 2 Major (wt.%), trace (ppm), and REE (ppm) element compositions of whole-rock samples from the Pingguo area, Guangxi[a)]

Sample No.	Lithology	Al_2O_3	SiO_2	CaO	K_2O	MgO	Na_2O	TiO_2	CIA	Li	Zr	Hf	Nb	Ta	La	Ce	Pr	Nd	Sm	Eu	Gd	Tb	Dy	Ho	Er	Tm	Yb	Lu	∑REE	Eu/Eu*	Nb/Ta	Zr/Hf
JM-01	Clastic bauxite	71.1	8.21	0.01	0.05	0.01	0.57	4.98	98.6	21.6	2032	44.4	216	7.27	4.45	14.2	0.71	2.6	0.99	0.23	1.23	0.32	2.48	0.53	1.51	0.26	2.04	0.27	31.8	0.65	29.7	45.8
M-02	Clastic bauxite	70.5	8.62	0.01	0.04	0.01	0.53	5.82	98.7	2.88	2243	47.8	238	8.73	4.65	14.2	0.69	2.36	0.89	0.2	1.1	0.28	2.18	0.46	1.37	0.23	1.91	0.24	30.8	0.61	27.3	46.9
JM-03	Clastic bauxite	70.1	9.78	0.01	0.04	0.01	0.46	5.17	98.9	5.75	2130	47.3	272	12.2	3.74	11.8	0.63	2.39	0.99	0.21	1.13	0.29	2.21	0.46	1.34	0.21	1.80	0.22	27.4	0.62	22.3	45
JM-04-2	Clastic bauxite	70.9	7.8	0.01	0.07	0.03	0.59	3.78	98.5	35.5	1588	33.6	193	9.25	3.76	11.6	0.66	2.27	0.88	0.19	1.11	0.29	2.31	0.47	1.36	0.21	1.74	0.22	27.1	0.61	20.9	47.3
JM-05	Pisolitic bauxite	73.5	6.22	0.01	0.04	0.02	0.40	4.79	99	6.85	1905	41.2	250	11.8	3.11	9.59	0.53	1.94	0.83	0.19	1.05	0.27	2.11	0.43	1.25	0.2	1.66	0.21	23.4	0.61	21.2	46.2
JM-06	Clastic bauxite	72.6	6.69	0.01	0.04	0.01	0.43	5.21	99	5.2	2069	43.8	261	9.92	4.85	15.1	0.94	3.34	1.19	0.25	1.38	0.34	2.56	0.53	1.55	0.25	2.01	0.27	34.6	0.61	26.3	47.2
JM-07	Carbonaceous clay rock	37.0	51.6	0	0.25	0.17	0.27	0.86	98.1	1639	660	17.4	36	2.38	4.3	9.34	0.6	1.65	0.51	0.12	0.76	0.23	1.92	0.42	1.23	0.19	1.32	0.18	22.8	0.61	15.5	37.9
JM-08	Carbonaceous clay rock	44.9	40.9	0.01	0.3	0.21	0.33	3.11	98.1	1211	1462	33	129	5.35	9.65	21.2	1.36	3.6	1	0.23	1.39	0.39	3.2	0.7	2	0.3	2.18	0.28	47.5	0.61	24.1	44.3
JM-08-2	Carbonaceous clay rock	3	54.3	0	0.27	0.16	0.33	0.96	97.7	1378	674	17.4	39.6	2.4	5.1	10.8	0.7	1.9	0.53	0.12	0.77	0.23	2	0.44	1.29	0.2	1.43	0.19	25.7	0.59	16.5	38.7
JM-08-3	Carbonaceous clay rock	41.5	45.4	0.01	0.29	0.14	0.70	1.84	96.6	1029	914	21.8	84.8	3.97	7.67	17.3	1.03	2.62	0.59	0.12	0.84	0.24	2.08	0.45	1.37	0.21	1.57	0.21	36.3	0.54	21.4	41.9
JM-09	Carbonaceous clay rock	39.7	40	0	0.56	0.41	0.32	1.49	97.2	2798	965	24.6	63.2	3.12	16.5	33.3	2.62	8.6	2.16	0.25	2.58	0.62	5.06	1.12	3.36	0.5	3.47	0.48	80.6	0.32	20.3	39.2
JM-10	Carbonaceous clay rock	39.8	41.8	0	0.42	0.24	0.33	1.4	97.6	1859.	816	20.1	58.1	2.80	18.2	34.8	2.27	6.47	1.4	0.2	1.9	0.52	4.57	1.08	3.37	0.53	3.7	0.53	79.5	0.38	20.8	40.6
JM-11	Carbonaceous clay rock	43.5	34.6	0.01	0.64	0.85	0.27	1.75	97.4	4886	894	20.9	60.6	3.09	21	42.6	2.98	9.26	2.22	0.29	2.88	0.74	6.27	1.46	4.52	0.7	4.81	0.69	100	0.35	19.6	42.8
JM-12	Carbonaceous clay rock	30.2	32.5	0.01	1.06	1.01	0.26	1.21	95	3790	929	20.6	43.1	2.49	19.7	51	5.39	22.8	7.79	0.61	8.57	1.91	14.4	3.23	9.73	1.5	10	1.48	158	0.23	17.3	45.1
JM-13	Carbonaceous clay rock	36.6	39.5	0.01	1.08	0.81	0.38	1.4	95.3	3623	843	19.7	45.7	2.76	24	45.2	3.58	12.2	3.25	0.31	3.9	0.91	7.45	1.76	5.58	0.88	5.96	0.87	116	0.27	16.6	42.8
JM-14	Carbonaceous clay rock	37.3	41.6	0	0.86	0.63	0.35	1.84	96.1	2846	928	21.5	65.7	3.5	20.3	29.3	2.46	7.58	1.8	0.22	2.32	0.58	5.15	1.29	4.08	0.64	4.4	0.63	80.7	0.34	18.8	43.2
JM-15	Carbonaceous clay rock	35.6	34.8	0.03	1.38	1.16	0.74	1.39	92.8	3388	818	18.6	61.9	3.27	19	35.6	3.5	13.9	4.26	0.36	4.9	1.16	9.42	2.23	7.05	1.11	7.65	1.12	111	0.24	18.9	44
XX-01	Limestone	0.1	0.05	55.7	0.01	0.27	0	0.01		4.3	17.2	0.43	3.18	1.41	9.57	12.8	1.66	7.35	1.61	0.32	2.02	0.35	2.4	0.52	1.39	0.19	1.03	0.15	41.4	0.55	2.26	40.4
XX-02	Limestone	0.1	0.1	54.9	0.01	0.43	0	0.01		2.29	8.38	0.2	1.15	0.2	7.47	13	1.68	7.71	1.84	0.34	2.12	0.37	2.5	0.55	1.52	0.20	1.22	0.18	40.7	0.54	5.87	43
XX-03	Limestone	0	0.1	55.6	0.01	0.47	0	0.01		1.78	4.28	0.07	0.58	0.12	0.46	0.5	0.08	0.33	0.07	0.02	0.09	0.02	0.11	0.03	0.08	0.01	0.07	0.01	1.86	0.62	4.98	64.9
XX-04	Iron-rich bauxite	54.7	1.67	0.19	0.02	0.02	0	2.73	99.9	7.49	1508	31.5	171	7.04	35.4	79.9	5.18	20.6	5.66	1.06	6.71	1.14	7.10	1.45	4.14	0.61	4.20	0.62	174	0.53	24.3	47.9
XX-05	Iron-rich bauxite	74.8	0.68	0.08	0.01	0	0	4.17	99.9	5.71	2283	47.6	250	10.2	25.1	79.6	3.90	12.5	1.93	0.32	2.67	0.56	4.11	0.9	2.76	0.45	3.34	0.48	139	0.43	24.5	48
XX-06	Pisolitic bauxite	79.5	0.91	0.05	0.01	0.01	0.01	4.22	99.9	4.56	2220	46.9	255	10.4	16.5	39.5	2.23	7.27	1.6	0.3	2.11	0.53	4.18	0.92	2.81	0.46	3.44	0.50	82.4	0.5	24.5	47.3
XX-07	Clastic bauxite	79.2	1.09	0.04	0.01	0	0.01	4.73	99.9	4.93	2482	54.3	279	11.7	20	49.3	2.17	6.17	1.21	0.24	1.86	0.5	4.31	0.98	3	0.50	3.84	0.54	94.6	0.49	23.9	45.7
XX-08	Pisolitic bauxite	79.0	1.34	0.06	0.01	0.01	0.01	4.74	99.9	5.86	2376	53.4	27	10.4	14.4	30.2	1.63	4.86	1.13	0.23	1.72	0.5	4.11	0.89	2.77	0.46	3.55	0.51	66.9	0.52	26.1	44.5
XX-09	Pisolitic bauxite	79.3	0.68	0.03	0.01	0	0	4.82	99.9	4.28	2397	54	271	10.3	14.8	30.3	1.73	5.54	1.31	0.26	1.89	0.53	4.35	0.92	2.8	0.46	3.55	0.51	68.9	0.51	26.3	44.4
XX-10	Pisolitic bauxite	78.9	1.06	0.02	0.01	0.01	0.01	4.13	99.9	7.75	2354	53.1	244	9.52	10.9	25.9	1.53	5.27	1.52	0.32	2.15	0.56	4.13	0.83	2.45	0.39	2.96	0.40	59.3	0.54	25.6	44.3
XX-11	Clastic bauxite	74.9	3.96	0.08	0.06	0.01	0.11	3.53	99.5	25.4	1961	43.9	206	8.63	7.99	22.1	1.34	4.69	1.54	0.32	1.94	0.45	3.17	0.64	1.85	0.29	2.18	0.29	48.78	0.57	23.9	44.7
XX-12	Carbonaceous clay rock	35.9	20.9	0.27	0.4	0.23	0.53	1.82	95.2	426	1155	22.7	83	4.09	50.3	133	11.8	45.8	12.3	1.48	11.5	2.34	16.3	3.27	9.48	1.41	9.62	1.39	310	0.39	20.3	50.9
XX-13	Carbonaceous clay rock	39.4	40.5	0.46	0.51	0.40	0.36	1.55	95.2	756	665	16.9	47.7	3.27	91.3	134	17.2	66	13.7	1.63	13.1	2.19	13.9	2.87	8.19	1.17	7.79	1.16	374	0.38	14.6	39.4
XX-14	Carbonaceous clay rock	39.5	44.9	0.25	0.26	0.08	0.42	0.55	96.5	292	258	8.67	32.2	2.89	13.1	20.4	1.93	6.25	1.14	0.15	1.22	0.22	1.51	0.34	1.07	0.18	1.26	0.19	49	0.40	11.1	29.8
XX-15	Carbonaceous clay rock	40.2	44.1	0.29	0.56	0.37	0.48	0.49	95.4	2214	274	10.2	35.4	2.91	8.65	21.3	2.35	9.01	2.03	0.31	1.85	0.33	2.16	0.45	1.28	0.19	1.35	0.19	51.5	0.49	12.2	26.9
XX-16	Carbonaceous clay rock	39.5	42.1	0.28	0.37	0.13	0.33	0.36	96.5	533	502	14.9	20.2	1.19	23.6	78.2	7.58	29.8	8.15	1.2	7.38	1.46	9.45	1.84	5.08	0.73	4.74	0.67	180	0.48	17	33.7

a) $Eu/Eu^*=Eu_N/(Sm_N \cdot Gd_N)^{1/2}$; chondrite data from Sun and McDonough (1989); $CIA=Al_2O_3/(Al_2O_3+CaO^*+Na_2O+K_2O) \times 100$, where CaO* can be estimated by assuming reasonable CaO/Na_2O ratios. If the CaO molar proportion is less than that of Na_2O, measured CaO can be used for CaO*; while CaO molar proportion is greater than that of Na_2O, CaO* is assumed to be equivalent to Na_2O (McLennan, 1993; Shao and Yang, 2012).

of kaolinite, goethite, pyrite, chloritoid, montmorillonite and zircon (Table 1; Figures 2 and 3). Diaspore particles exhibit short prismatic or platy shapes, usually 10–50 μm in size, with some exceeding 100 μm (Figure 2a–2c, 2e–2f). Anatase particles are typically small (<1 μm), although some occur as automorphic or hypautomorphic granules (>5 μm), with some appearing as spindle-shaped anatase aggregates, which may indicate that the anatase was formed from titanium minerals (such as ilmenite) that retained their original mineral outlines (Figure 2c–2d). Pyrite often exists as aggregates, in the form of automorphic and hypautomorphic granules, indicating a typical sedimentary origin (Figure 2a and 2e). Small numbers of kaolinite grains are present, and are lamellar and flexible (Figure 2d). The clay rocks contain a variety of minerals, including pyrophyllite, cookeite, illite, kaolinite, and diaspore. In addition, some clay rocks contain small amounts of dickite, goethite, and pyrite (Table 1; Figure 2). The pyrophyllite exhibits leaf-shaped morphologies, has the largest grain size among clay minerals (usually >20 μm), and typically occurs on the edges of diaspores, indicating a close genetic relationship between the two (Figure 2f). The cookeite forms fine, scaly-shaped particles

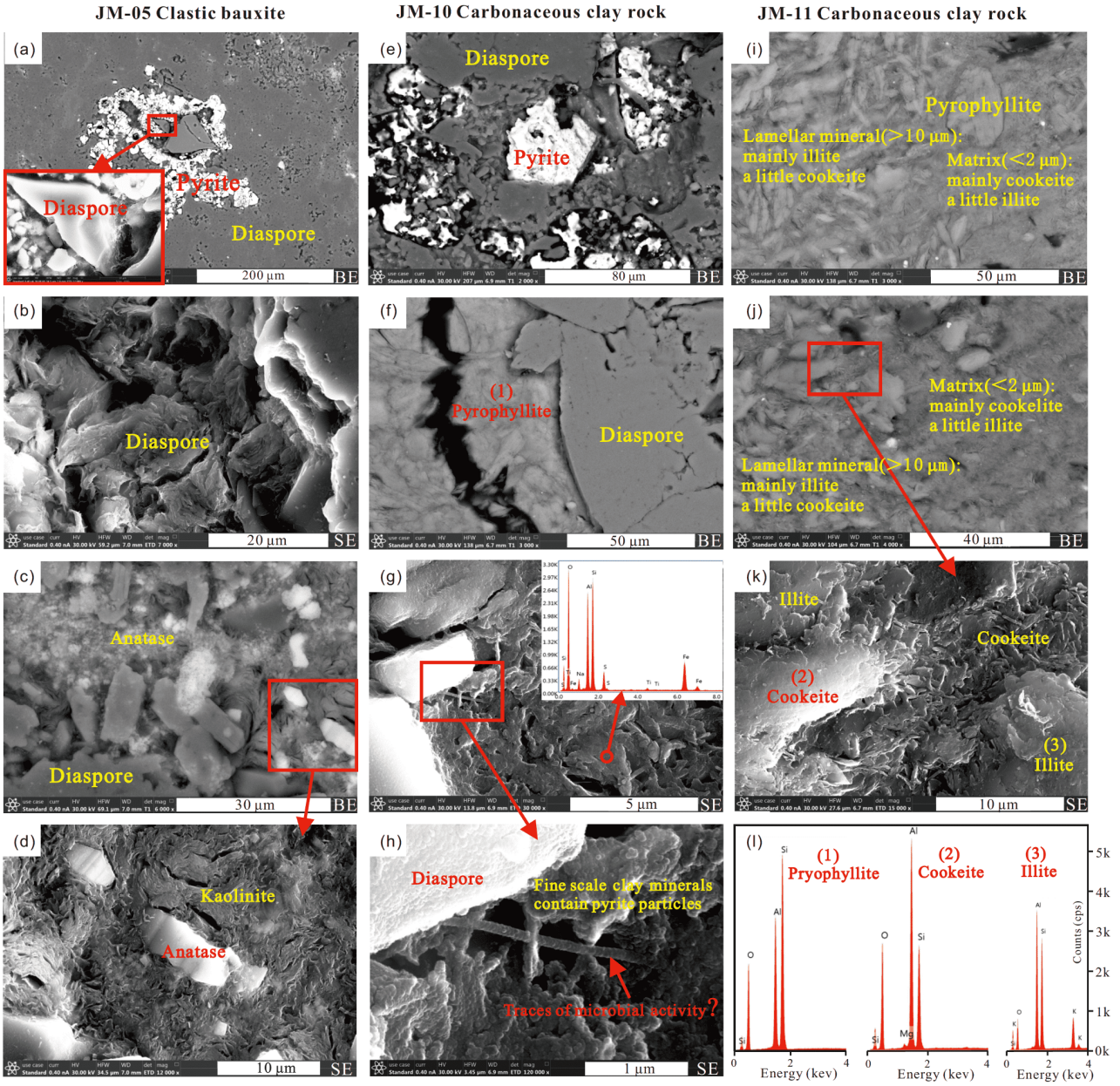

Figure 2 SEM images of bauxite and clay rocks from the Heshan Formation. (a) Authigenic pyrite and platy diaspore; (b) platy diaspore; (c) coexisting anatase and diaspore; (d) anatase particles distributed randomly in kaolinite matrix; (e) coexisting diaspore and pyrite; (f) pyrophyllite on the edges of diaspores; (g) EDS analysis showing dickite/kaolinite and a small amounts of pyrite; (h) traces of microbial activity; (i) cookeite, illite, and pyrophyllite coexisting; (j) cookeite and illite coexisting; (k) cookeite and illite coexisting; (l) EDS patterns of selected pyrophyllite, cookeite, and illite. BE, backscattered electron image; SE, secondary electron image.

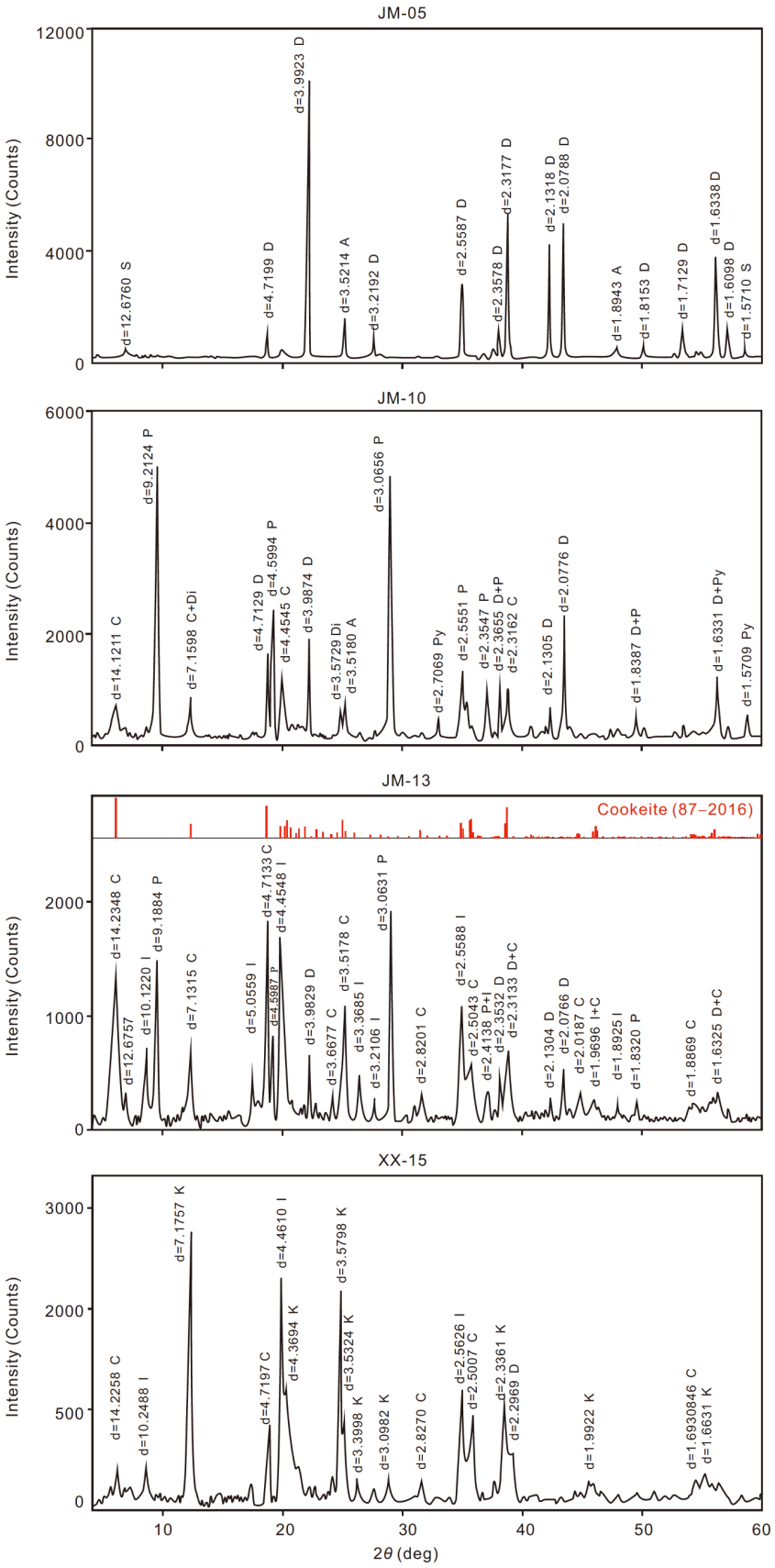

Figure 3 (Color online) XRD patterns of selected samples from the Heshan Formation in Pingguo, Guangxi. D, diaspore; A, anatase; S, stilpnomelane; C, cookeite; I, illite; Di, dickite; Py, pyrite; K, kaolinite.

(<2 μm), rarely exhibits platy morphologies (>10 μm), and usually coexists with illite and pyrophyllite. In contrast, illite and pyrophyllite primarily show lamellar morphologies (>10 μm) (Figure 2i–2k). In addition, fine grained clay minerals (10–100 nm) and traces of microbial activity in JM-10 indicate that microorganisms were involved in the formation of these clay minerals. According to the EDS analysis, the mineral composition of JM-10 includes dickite or kaolinite, with a small amount of pyrite that may be related to bacterial sulphate reduction (Figure 2g and 2h).

As clay minerals in sedimentary rocks are small and commonly xenomorphic, it is difficult to identify them on the basis of morphological characteristics alone. Based on the semi-quantitative analysis (XRD) of the minerals, SEM-EDS analysis can be used to identify clay minerals more accurately according to the differences in their chemical components. For example, illite ($K_{0.7}Al_2[(Si,Al)_4O_{10}](OH)_2$) and montmorillonite ($(Ca,Na)_{0.33}(Al,Mg)_2(Si_4O_{10})(OH)_2\cdot nH_2O$) contain relatively high contents of K and Mg, respectively, which distinguishes them from other clay minerals. Kaolinite ($Al_4[Si_4O_{10}](OH)_8$) and pyrophyllite ($Al_2[Si_4O_{10}](OH)_2$) can be identified based on the difference in their Al:Si atomic ratios of 1:1 and 1:2, respectively (Figure 2l). Although Li cannot be analysed via EDS due to the low energy of its characteristic X-ray spectrum, the identification of cookeite ($LiAl_4(Si_3AlO_{10})(OH)_8$) is possible based on its unique Al:Si ratio of 5:3, which is different from other clay minerals (Figure 2l). In addition, chamosite (rich in Fe) and clinochlore (rich in Mg) can also be readily distinguished from cookeite because it contains trace Fe and Mg.

4.2 Geochemical composition

The bauxite has relatively high Al_2O_3 (54.7–79.5 wt.%, average 73.5 wt.%) and TiO_2 (2.73–5.82 wt.%, average 4.49 wt.%) contents, and comparatively low SiO_2 (average 4.19 wt.%), CaO (average 0.04 wt.%), MgO (average 0.01 wt.%), Na_2O (average 0.22 wt.%), and K_2O (average 0.03 wt.%) contents. High chemical index of alteration (CIA) values of 98.5–99.9 (average 99.4) indicate that the bauxite has experienced strong chemical weathering and water-rock interaction, resulting in the loss of mobile elements, preserving only those immobile elements such as Al and Ti (Table 2; Figure 4). The clay rocks have moderate Al_2O_3 (30.2–44.9

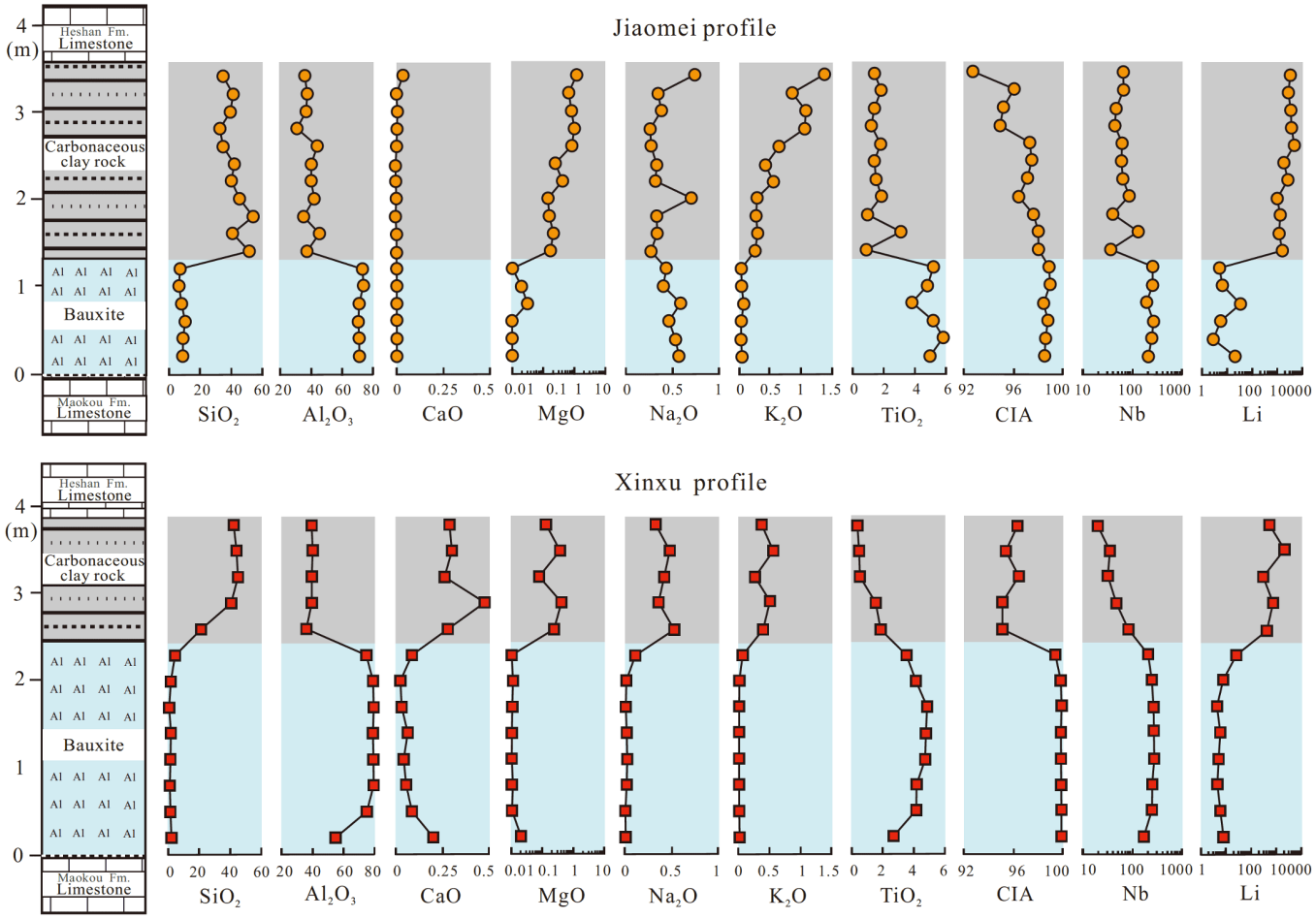

Figure 4 (Color online) Concentrations of selected elements and CIA values for the Jiaomei and Xinxu profile samples.

wt.%, average 38.5 wt.%) and SiO_2 (20.9–54.3 wt.%, average 40.6 wt.%) contents. CaO (average of 0.1 wt.%), MgO (average of 0.44 wt.%), Na_2O (average of 0.4 wt.%), and K_2O (average of 0.58 wt.%) contents are generally low, but higher than those of bauxite. The CIA values of the clay rocks are also high (92.8–98.1, average 96.3) and the MgO and K_2O contents are 10–50 times higher than those of bauxites, indicating that the clay rocks also experienced strong to moderate chemical weathering (Table 2; Figure 4). Other than CaO (average of 55.4 wt.%), the MgO (average of 0.39 wt.%) and other element contents in the Maokou Formation limestone are fairly low (Table 2).

The Heshan Formation sedimentary rocks in Pingguo are rich in critical metals, with bauxite rich in Nb and Zr, and clay rocks rich in Li (Table 2; Figure 4). The Li concentration in clay rocks in the Jiaomei section ranges from 1029 to 4886 ppm (average 2586 ppm; Li_2O=0.56 wt.%), which exceeds the cut-off grade for clay-type Li deposits abroad (Li > 1000 ppm) and that of China's hard-rock Li ores (Li_2O=0.5 wt.%; Figure 5a; Wang et al., 2012b, 2013; Castor and Henry, 2020). The clay rocks in the Xinxu section exhibit slightly lower Li concentrations than that of Jiaomei section, ranging from 292 to 2214 ppm (average 892 ppm; Table 2). In comparison, the Li content in the bauxite is relatively low, ranging from 2.88 to 35.5 ppm (average 10.3 ppm; Table 2; Figures 4 and 5a). The concentration of Zr and Nb are extremely high in the bauxite, with Zr in the range of 1508–2482 ppm (average 2111 ppm) and Nb content in the range of 171–279 ppm (average 241 ppm), which exceeds the lowest industrial grade for weathering crust Nb (tantalum) deposits (100–120 ppm; Nb_2O_5=0.016–0.02 wt.%; Table 2; Figures 4 and 5b). The clay rocks contain moderate Nb concentrations, ranging from 20.1 to 129 ppm (average 56.7 ppm), and Zr concentrations range from 258 to 1462 ppm (average 797 ppm; Table 2; Figures 4 and 5b). The REE contents in the bauxite are relatively low, ranging from 23.4 to 174 ppm (average 64.9 ppm); in the clay rocks, they are relatively enriched, ranging from 22.8 to 374 ppm (average 114 ppm; Table 2). The bauxites and clay rocks have average Eu/Eu* values of 0.56 and 0.41, respectively, and have strongly negative Eu anomalies (Table 2).

5. Discussion

5.1 Nb and Li occurrence

TiO_2-rich minerals, including anatase and rutile, were either inherited from the parent rock or came from the transformation of Ti-rich minerals such as ilmenite in the parent rocks through weathering and sedimentation. They are typically the main carrier minerals of Nb in sedimentary rocks (Mordberg et al., 2001; Liu et al., 2013). Mineral analysis reveals that the anatase content in the Heshan Formation, especially in the bauxite, is relatively high (Table 1; Figure 2c and 2d), and the content of anatase and TiO_2 is significantly positively correlated with the whole-rock Nb content. This indicates that anatase is the main carrier mineral of Nb, which is consistent with previous studies (Figure 6a and 6b; Hou et al., 2017). The positive correlation of Al_2O_3 vs. Zr (Figure 6c) and Al_2O_3 vs. TiO_2 content (Figure 6d) implies that, as the degree of weathering increased, the amount of mobile elements decreased, and the amount of immobile elements such as Al, Ti, Nb, and Zr increased, eventually resulting in the formation of the Nb-Ti-Zr-rich bauxite layer in the Heshan Formation (Figure 6c and 6d).

The results of the XRD and SEM-EDS analyses show that Li-rich clay rocks contain large quantities of cookeite, and whole-rock Li contents are positively correlated with cookeite contents (R^2=0.81). The Li/cookeite ratio is 0.0069–0.0237 (average 0.0127), which is close to the theoretical value (0.0133) of the Li content in cookeite. This indicates that cookeite is the main carrier mineral of Li (Table 1; Figure 3 and 7a). Super-enrichment of Li and similar mineral assemblages (mainly kaolinite, illite, cookeite, pyrophyllite,

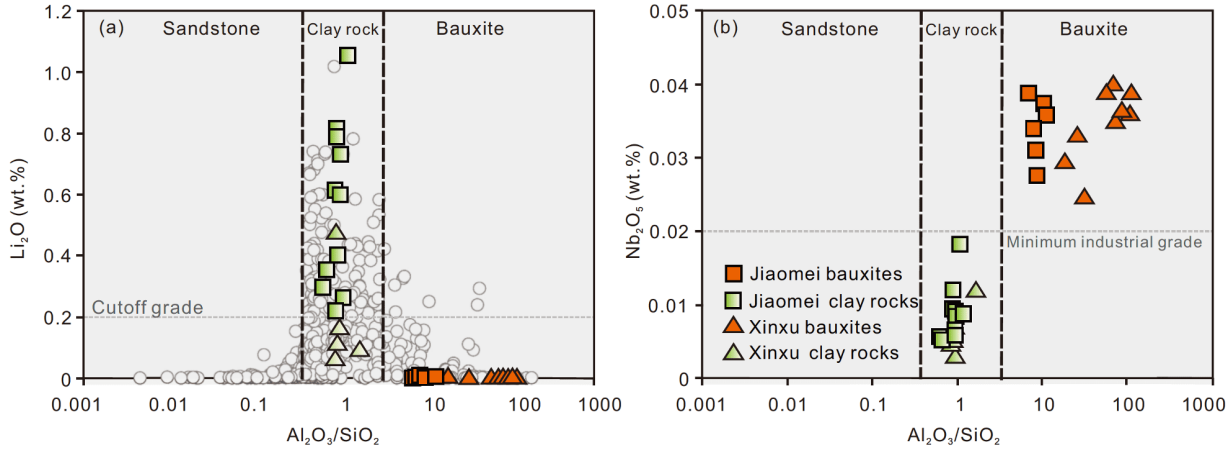

Figure 5 (Color online) Bivariate plots of Al_2O_3/SiO_2 vs. Li_2O (a) and Al_2O_3/SiO_2 vs. Nb_2O_5 (b). Open circles are data from Wen et al. (2020).

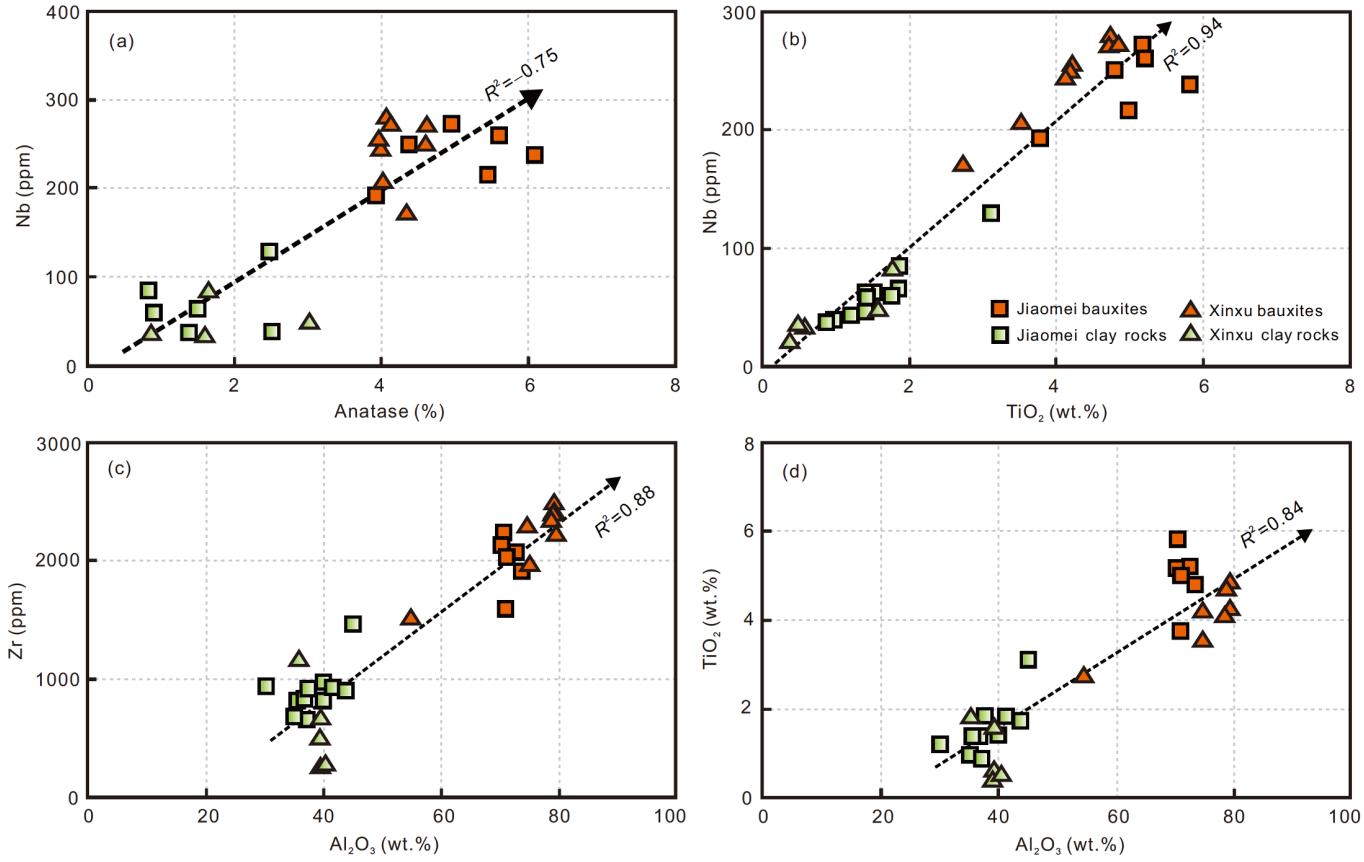

Figure 6 (Color online) Bivariate plots of anatase vs. Nb (a), TiO_2 vs. Nb (b), Al_2O_3 vs. Zr (c), and Al_2O_3 vs. TiO_2 (d).

dickite, and diaspore) have also been described in the bauxite ore-bearing rock of the Upper Carboniferous Benxi Formation in Henan Province, referred to as "cookeite clay rock" (Shen et al., 1986; Song et al., 1987). The significant positive correlation between whole-rock MgO and Li contents in the Li-rich clay rocks in Pingguo (R^2=0.85) may be the result of the substitution of Li and Mg in clay minerals, owing to their similar radii and chemical properties (Li^+=0.76 Å and Mg^{2+} =0.72 Å).

In summary, the Heshan Formation bauxite contains a large amount of anatase, and the anatase content positively correlates with whole-rock TiO_2 and Nb contents (Figure 6a and 6b), indicating that the Nb is mainly hosted in the anatase. The clay rocks contain abundant cookeite, which exhibits a significant positive correlation with Li content, thus indicating that cookeite is the main host mineral for Li.

5.2 The genesis of cookeite

Before the 1960s, it was believ that pyrophyllite, dickite, and chlorite form in mineral veins and hydrothermal alteration zones associated with metamorphic rocks and hydrothermal activity (Fu et al., 2012). Further research has shown that these minerals are also present in sedimentary rocks such as coal, sandstone, sedimentary iron ores and clay rocks, indicating they can also formed in supergene systems (Ehrenberg et al., 1993; McAulay et al., 1993; Lanson et al., 2002).

In the present study, the cookeite might have formed through the alteration of pyroclastic materials (such as volcanic ash), because the Heshan Formation in Guangxi might have been derived from the ELIP and Permian Paleo-Tethyan magmatic arc (Deng et al., 2010; Yu et al., 2016; Hou et al., 2017). Clay rocks formed by hydrothermal alteration usually have a low degree of chemical weathering along with high levels of potassium, sodium, and quartz (Gao et al., 2016). For example, the McDermitt (Nevada, USA) clay-type Li deposit is located in a Cenozoic caldera, and its ore mineral hectorite was derived from the transformation of Li-rich pyroclastic materials in response to hydrothermal activity. The ore exhibits a porous texture, with a low degree of weathering (CIA average 53.3), high SiO_2 contents averaging 73.7 wt.%, CaO contents averaging 2.05 wt.%, MgO contents averaging 3.24 wt.%, Na_2O contents averaging 2.46 wt.%, and K_2O contents averaging 3.27 wt.% (Benson et al., 2017; Castor and Henry, 2020). These characteristics are markedly different from the Li-rich clay rocks in Pingguo, which has a high degree of weathering (CIA average 96.3), low K_2O contents averaging 0.58 wt.%, Na_2O contents averaging 0.4 wt.%, CaO contents averaging 0.1 wt.% and

MgO contents averaging 0.44 wt.%. This indicates that the Li-rich clay rocks and cookeite in Pingguo were formed through weathering and subsequent deposition, rather than by hydrothermal alteration (Tables 1 and 2).

In sedimentary rocks, clay minerals may be transported as detritus or formed by secondary processes during diagenesis, such as solution precipitation and transformation from other minerals (He, 2001; Ouahabi et al., 2017; Fang et al., 2019). During continental weathering, the dissolution of primary minerals results in the loss of mobile elements such as K, Na, Ca, Mg, Sr, and Li, whereas immobile elements such as Al, Si, and Fe remain to form different assemblages of clay minerals and oxides, which can be used to measure the intensity of continental weathering (Setti et al., 2014; Fang et al., 2019; Yu et al., 2019). For example, chlorite often exists in arid and cold areas dominated by physical weathering, but with weak chemical weathering. In contrast, the presence of kaolinite and bauxite indicates warm and humid climate conditions and strong chemical weathering (Setti et al., 2014; Vögeli et al., 2017). The average CIA values of the Pingguo bauxite and clay rock samples are 99.4 and 96.3, respectively, indicating intense chemical weathering. Therefore, the presence of cookeite in the clay rocks can be attributed to transformation from other minerals during diagenesis, rather than to an autogenic origin (Table 2; Thiry, 2000).

It is largely held that cookeite discovered in bauxite ores has been transformed from other clay minerals during diagenesis (Vrublevskaja et al., 1975; Shen et al., 1986; Song et al., 1987). For example, cookeite, pyrophyllite, and diaspore coexist in the bauxite deposits of the Djalair area, Central Asia, where there is evidence of mineral phase transformations: A large amount of cookeite present in the fractures of pyrophyllite indicate that cookeite was transformed from pyrophyllite (Vrublevskaja et al., 1975). In addition, the cookeite in the clay rocks from Henan has been considered as transformed from illite (Shen et al., 1986). In the clay rocks of Pingguo, cookeite, illite and pyrophyllite coexist and are closely related (Figure 2i–2k). Furthermore, the pyrophyllite content shows a significant negative correlation with cookeite content (R^2=−0.95) and illite content (R^2=−0.94), indicating that the cookeite might have formed through the reaction of pyrophyllite or illite with a Li-rich solution (Figure 7c–7d).

5.3 Provenance of the upper Permian Heshan Formation in Pingguo, Guangxi

Previous studies on the provenance of the Heshan Formation in western Guangxi focused mainly on the bauxite source in the lower layer (e.g., MacLean et al., 1997; Wang et al., 2012a). In the last century, on the basis of mineral and elemental geochemical affinities (e.g., Al_2O_3/TiO_2, REE pat-

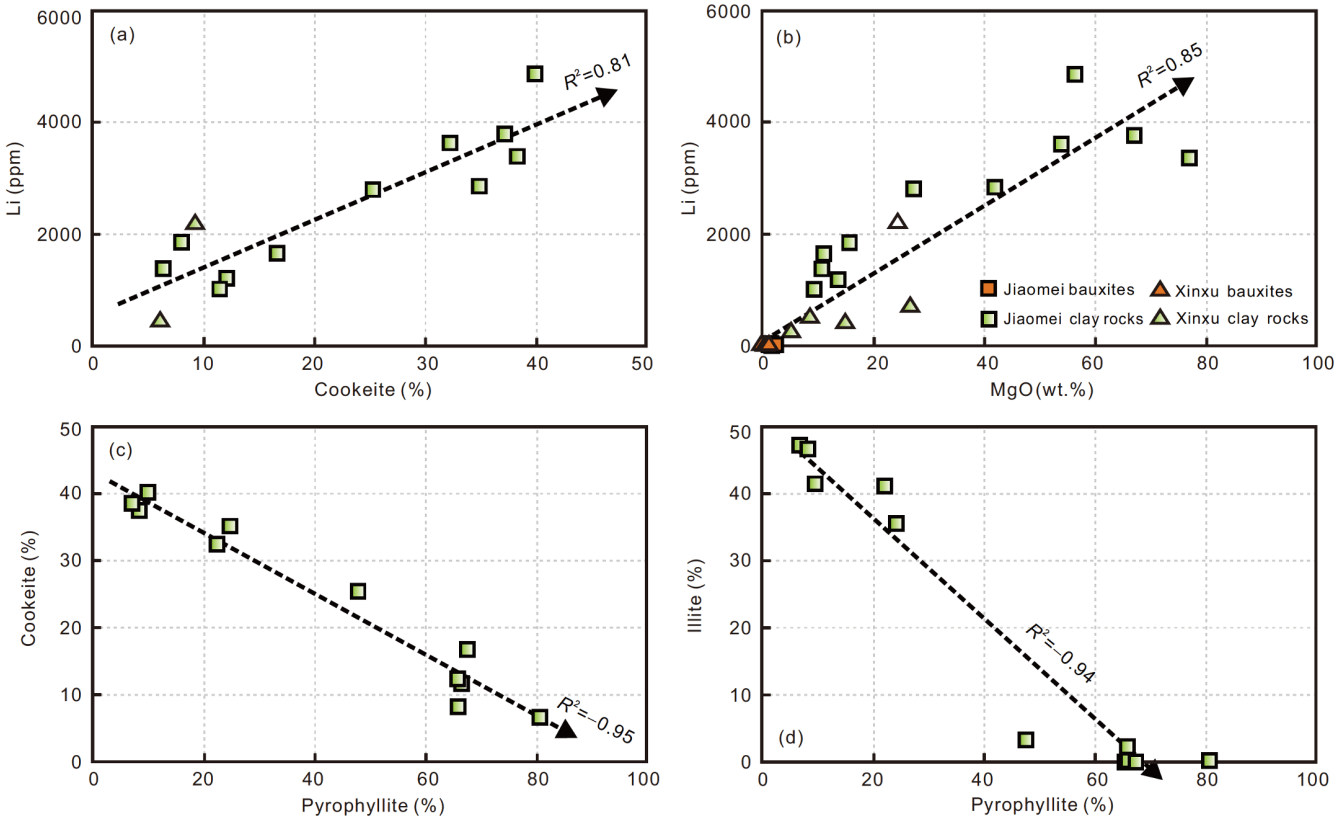

Figure 7 (Color online) Bivariate plots of cookeite vs. Li (a), MgO vs. Li (b), pyrophyllite vs. cookeite (c) and pyrophyllite vs. illite (d).

terns), the Maokou Formation limestone has been considered an important source of bauxite (Dai et al., 2007). However, carbonate rocks usually have low Al_2O_3 content (< 0.5 wt.%) and were not considered to be the main sources of the bauxites (Yin, 2009; Yu et al., 2014). For instance, the Al_2O_3 contents of three samples of the Maokou Formation limestone from Pingguo are less than 0.1 wt.%, which is much lower than those of igneous and clastic rocks (Table 2). In recent years, with the rapid development of *in situ* zircon analysis, detrital zircon provenance tracing has facilitated significant progress in the study of bauxite provenance. Detrital zircon studies on the Heshan Formation over multiple areas of western Guangxi yield consistent results, with a single age peak (ca. 260 Ma) and a negative Hf isotope composition, which indicate sources mainly in the ELIP- or Permian magmatic arc-related felsic rocks (Deng et al., 2010; Yu et al., 2016; Hou et al., 2017). Zircons are largely produced in felsic rocks and rarely seen in mafic rocks. Although the detrital zircon studies noted above indicate a source of felsic rocks, mafic rock sources cannot be neglected (Hou et al., 2017). The abundant and widely distributed basalt in the ELIP might represent one of the sources of the Heshan Formation, but this is yet to be confirmed via detrital zircon analysis. Therefore, other methods are required to elucidate the provenance of the Heshan Formation.

5.3.1 Provenance analysis of immobile elements

Immobile elements such as Nb, Ta, Zr, Hf, Ti and Al are usually stable during supergenetic and hydrothermal alteration, and Al_2O_3/TiO_2, Zr/Hf, and Nb/Ta ratios have proven effective in tracing the provenance of sedimentary rocks (Zhong et al., 2013; Dai et al., 2014; Zhang et al., 2016). The Al_2O_3/TiO_2 ratios of mafic, intermediate, and felsic rocks range from 3 to 8, 8 to 21, and 21 to 70, respectively (Hayashi et al., 1997). The bauxites and clays of the Heshan Formation in Pingguo plot within the field of intermediate and felsic rocks in Al_2O_3/TiO_2 diagram, respectively (Figure 8a). On the Al_2O_3/TiO_2-Eu/Eu* plot, most samples lie within the peralkaline felsic rock field (Figure 8b), with a few clay rock samples plotting within the peraluminous felsic rock field. The bauxite appears to have formed primarily from alkaline felsic rocks, whereas the clay rocks have a mixed origin in peralkaline and peraluminous felsic rocks. Bivariate diagrams of CIA-Al_2O_3 and Zr/Hf-Zr show that the bauxites and clay rocks have completely different evolutionary trends and that their source rocks are distinct (Figure 8c–8d).

In sedimentary rocks, Zr and Hf mainly occur in zircon, whereas Nb and Ta primarily occur in anatase (Zhao et al., 2008; Chen and Yang, 2015). Therefore, the whole-rock Zr/Hf and Nb/Ta values essentially represent the values of zircon and anatase, respectively, for effective provenance tracing (Ballouard et al., 2016; Wu et al., 2017). The bauxite

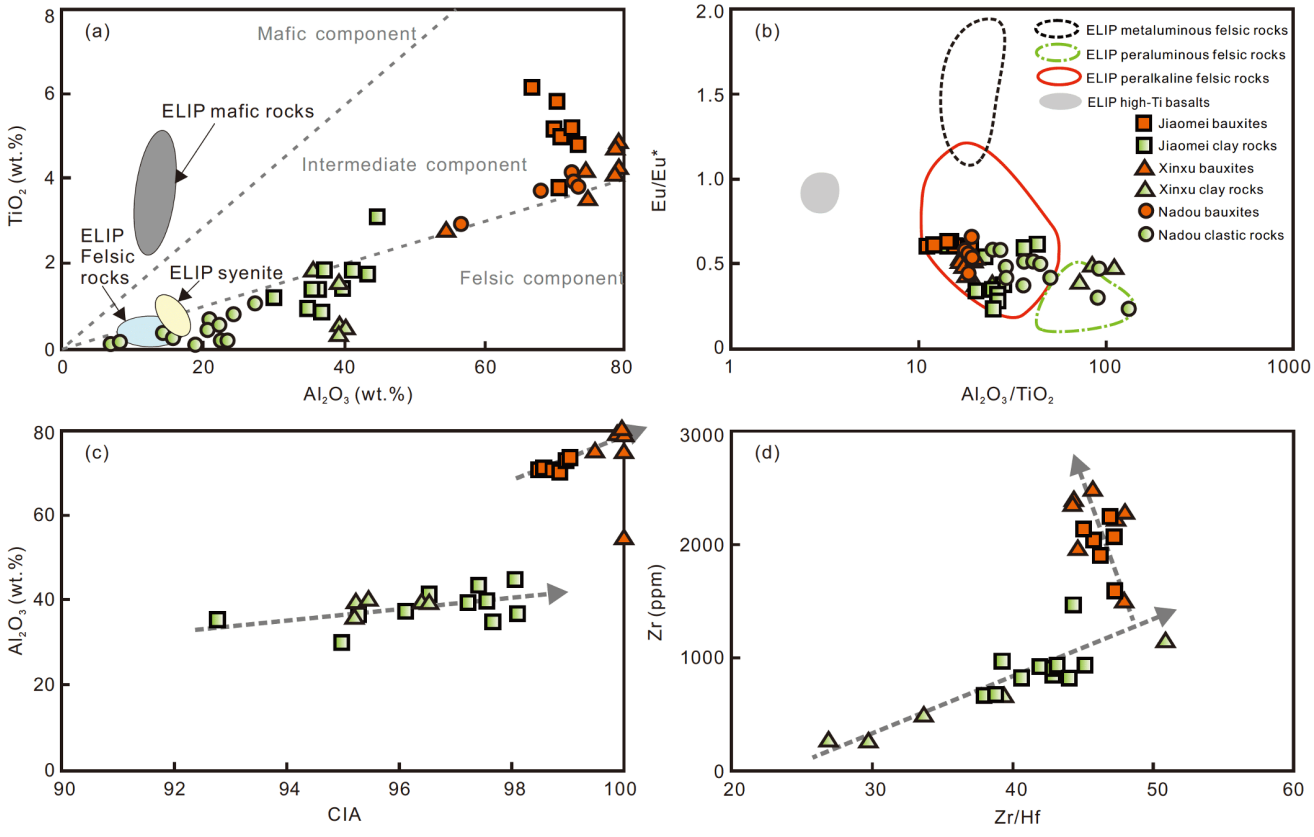

Figure 8 (Color online) Bivariate plots of Al_2O_3 vs. TiO_2 (a), Al_2O_3/TiO_2 vs. Eu/Eu* (b), CIA vs. Al_2O_3 (c) and Zr/Hf vs. Zr (d).

and clay rocks in the Heshan Formation differ significantly in terms of their Nb/Ta ratios, indicating an abrupt change in provenance. The Nb/Ta ratio of bauxite ranges from 20.9 to 29.7, with an average of 24.8, which exceeds the value for chondrite (19.9; Münker et al., 2003) and plots within the field for alkaline felsic rocks and A_1-type granitoids (Figure 9). In contrast, the average Nb/Ta ratio for the clay rocks is 17.8, close to that of upper continental crust (UCC=13–15). The clastic rocks in the Nadou profile have a very low Nb/Ta ratio (4.3–16, average 9.8), and plot within the fields of peraluminous felsic rock and A_2-type granitoids in Nb-Nb/Ta diagram (Figure 9; Green, 1995; Hou et al., 2017).

Generally, the Nb/Ta ratios of silicate reservoirs on Earth are lower than that of chondrite (19.9), a phenomenon known as the "mysterious disappearance of Nb" (Münker et al., 2003; Tang et al., 2019). Rocks with higher Nb/Ta values than chondrite are mainly alkaline rocks, basic dike swarms, Archean Tonalite-Trondhjemite-Granodiorite (TTG), and Archean mafic volcanic rocks (Zhao et al., 1999). As noted above, the source of the bauxites in the Heshan Formation is closely associated with the ELIP or the Permian Paleo-Tethyan magmatic arcs, thus excluding provenance contributions from Archean TTG and Archean mafic rocks. The small ELIP basic dike swarms that are largely developed in the inner-intermediate zone rather than the outer zone of the ELIP cannot be the major source of the large-scale bauxite deposits in western Guangxi (Li et al., 2010). Alkaline rocks generally form in a non-orogenic environment (Eby, 1992; Zhao et al., 2008), suggesting a possible contribution from the ELIP. Alkaline felsic rocks in the ELIP, such as A_1-type granite and syenite with Nb/Ta ratios higher than that of chondrite are the most likely source for the bauxite deposits in western Guangxi (Zhou et al., 2005). For example, the Baima alkaline syenite and some syenites and A_1-type granites in Ailanghe, Cida, and Taihe, in the Panxi area are characterized by high Nb/Ta ratios, averaging 20.3 with a maximum of 26.8 (Shellnutt and Zhou, 2008; Zhong et al., 2007, 2009, 2011). Alkaline felsic rocks such as A_1-type granite are usually enriched in Zr, Hf, Nb, Ta and other incompatible elements, but lacking in Ni, Co, Sc, Ba and Sr (Eby, 1992; Nyman et al., 1994), which is consistent with the enrichment of Zr, Hf, Nb and Ta in the Heshan Formation bauxite, indicating that the ELIP alkaline felsic rocks are a possible source. In the bivariate diagram of Zr/Hf-Nb/Ta (Figure 10), Pingguo bauxites fall within the field of ELIP alkaline rocks and A_1-type granite. Conversely, the clay rocks are located within the field of peraluminous granite (including A_2-type granite) or moderately fractionated granite, and are consistent with the distribution of the intermediate-felsic rocks of the Permian magmatic arc. The

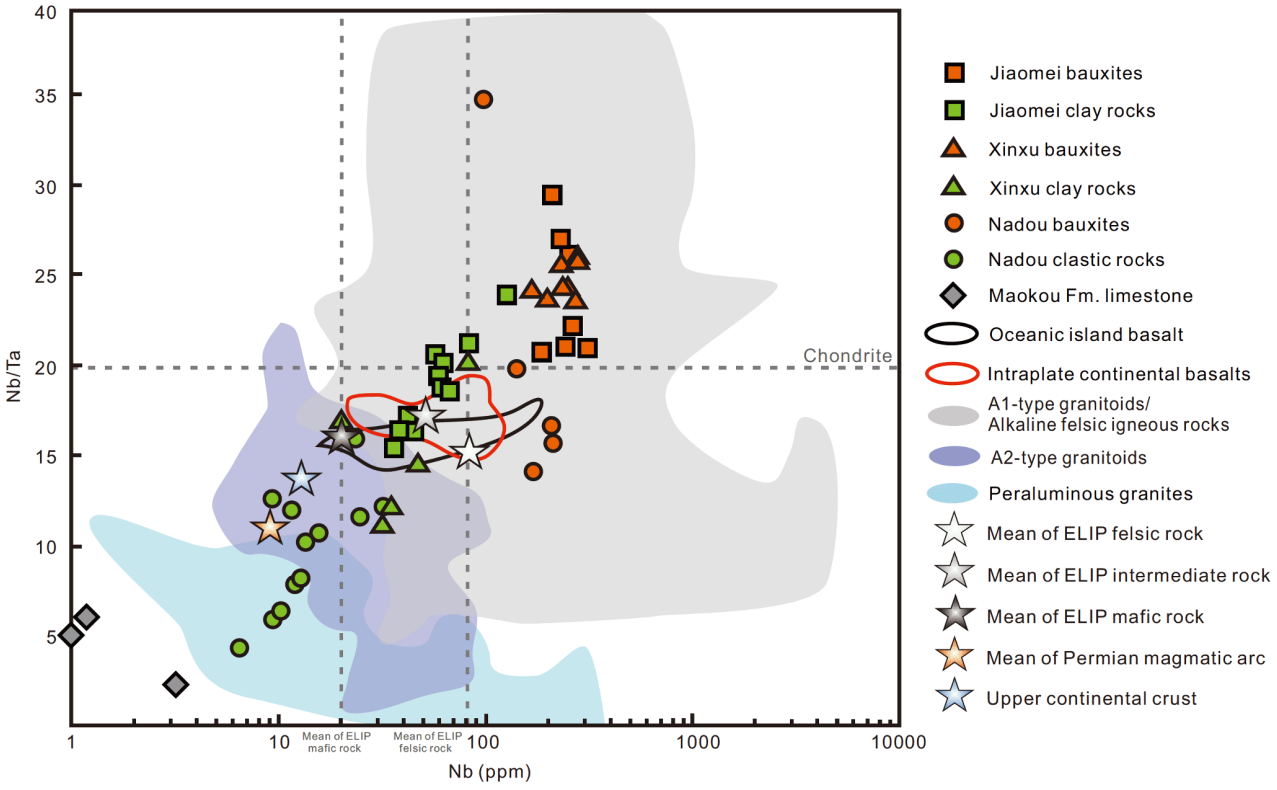

Figure 9 Bivariate plots of Nb vs. Nb/Ta for samples of the Heshan Formation. Background data fields are from Ballouard et al. (2020); Nadou data are from Hou et al. (2017); UCC data are from Münker et al. (2003); ELIP data are from Xu et al. (2001, 2010), Xiao et al. (2004), Shao et al. (2007), Shellnutt and Zhou (2007, 2008), Shellnutt and Jahn (2010), and Zhong et al. (2007, 2009, 2011); Permian igneous arc data are from Hoa et al. (2008) and Halpin et al. (2016).

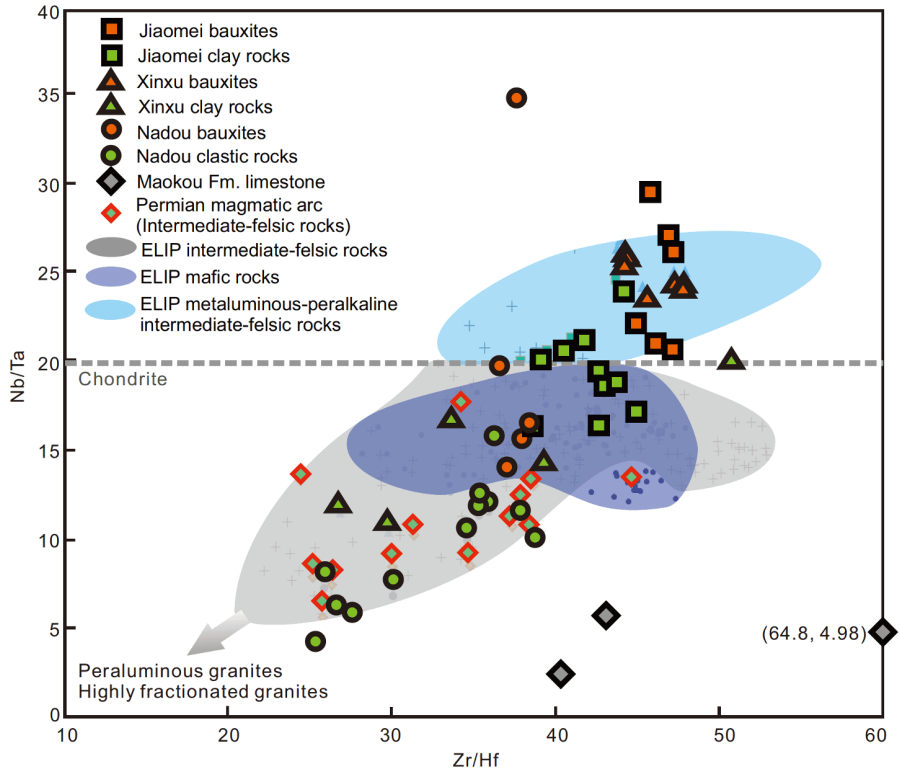

Figure 10 Bivariate plots of Zr/Hf vs. Nb/Ta. Nadou data are from Hou et al. (2017). Sources of ELIP and Permian igneous arc data are the same as those in Figure 9.

Nb-Nb/Ta relationship in the clay rocks of the Heshan Formation in Pingguo also shows a close resemblance to that of the Permian Paleo-Tethyan magmatic arc (Figure 9), indicating that those rocks are a potential source.

5.3.2 *Provenance analysis of rare earth elements*

Mafic and ultramafic rocks generally exhibit weak negative or no Eu anomalies, whereas felsic rocks show strongly negative Eu anomalies. These characteristics, which may be preserved in sedimentary rocks, can be used as provenance indicators (Taylor and McLennan, 1985; He et al., 2007). The chondrite-normalized REE pattern of the Heshan Formation in Pingguo is similar to that of felsic rocks (Figure 11). In particular, the clay rocks from the Jiaomei section show strongly negative Eu anomalies, which are similar to those of peraluminous and highly fractionated granites (Chen and Yang, 2015; Wu et al., 2017). Furthermore, the bauxite and clay rocks of the Heshan Formation exhibit a significant REE tetrad effect (groups 3 and 4; Figure 11), which has been observed in only a few natural materials to date. For example, some marine organisms, shells and corals, and shallow groundwaters exhibit a W-type tetrad effect, whereas some granite, alkaline rocks and detrital materials yield an M-type tetrad effect (Masuda et al., 1987; Takahashi et al., 2002; Feng et al., 2011). The M-type tetrad effect is prevalent in granites, particularly highly fractionated and peraluminous types, and in alkaline rocks from South China, Xinjiang Province, and other regions (Zhao et al., 1992; Wu et al., 2011; Ballouard et al., 2016).

Highly fractionated and peraluminous granites usually show strong Eu depletion because of high degrees of separation and crystallization. This results in extreme enrichment of volatile and alkali metals, rare metals, and REEs, and finally results in fluid-melt coexistence and interactions leading to the formation of an M-type REE tetrad effect in the melt phase (Zhao et al., 1999). For example, lepidolite granite with rare metal mineralization in the Erzgebirge region of Europe shows a significantly negative Eu anomaly and REE tetrad effect (Förster et al., 1999; Ballouard et al., 2020). The clay rocks of the Heshan Formation exhibit strongly negative Eu anomalies and an M-type tetrad effect, indicating that they might have originated from peraluminous or highly fractionated felsic rocks. The bauxite deposits exhibit moderately negative Eu anomalies and an M-type tetrad effect, indicating a close relationship with alkaline felsic rocks (e.g., A_1-type granite, syenite, trachyte).

5.3.3 *Abrupt change in source for the bauxite and clay rock*

The Nb-Nb/Ta and Zr/Hf-Nb/Ta relationships for the Maokou Formation limestone are markedly different from those of the Heshan Formation in Pingguo. Although their REE patterns share certain similarities, differences include a negative Ce anomaly and a reduced negative Eu anomaly for

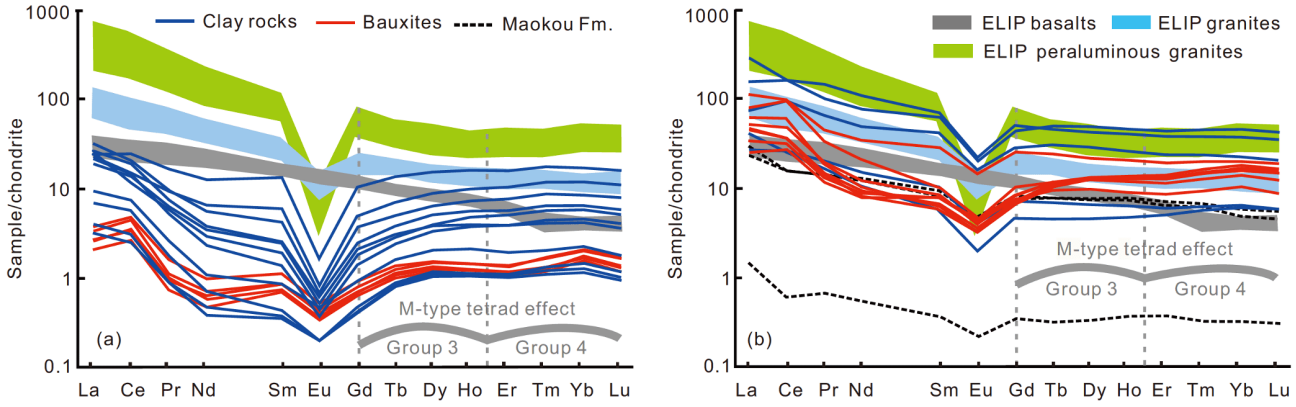

Figure 11 Chondrite-normalized REE patterns of the Jiaomei section (a) and the Xinxu section (b). Normalized values are from Sun and McDonough (1989). Data for ELIP basalts and granites are from Xu et al. (2001) and Xiao et al. (2004), and those for ELIP peraluminous granites are from Zhong et al. (2007).

the Maokou Formation, indicating it is not the major source of the Heshan Formation (Figures 9–11; Deng et al., 2010; Yu et al., 2016; Hou et al., 2017). Provenance analyses using Al_2O_3/TiO_2, Nb/Ta, Zr/Hf, and REEs reveal that the source of the Heshan Formation clastic rocks lies mainly in intermediate-felsic rocks, with a small contribution from the Maokou Formation limestone and ELIP basalts. Moreover, the provenances of the Nb-rich bauxite and the overlying Li-rich clay rocks are distinct. The Nb-rich bauxite in the lower Heshan Formation was derived from the weathering of ELIP alkaline felsic rocks (e.g., A_1-type granitoids, alkaline syenite, and trachyte), whereas the source of the overlying Li-rich clay rocks are peraluminous or moderately fractionated felsic rocks in the Permian Paleo-Tethyan magmatic arc (Figure 1a). Similar abrupt changes in provenance have been observed in the Xuanwei, Longtan (eastern Yunnan, southern Sichuan, western Guizhou, and Chongqing), and Linghao (western Guangxi) formations overlying ELIP basalts (Figure 1c; Huang et al., 2014). In addition, the lowermost Xuanwei Formation and Longtan Formation are also rich in critical metals, such as Nb(Ta), Zr(Hf), Ga and REEs, and are referred to as polymetallic layers (Figure 1c; Dai et al., 2010; Zhao and Graham, 2016; Zhao et al., 2016, 2017). The discovery of Nb-rich bauxite in the lower Heshan Formation expands the Nb-rich polymetallic layer occurrence from the intermediate zone to the outer zone (Pingguo area, Guangxi) of the ELIP. This finding has improved the understanding of ELIP distributions and related mineralization (Figure 1c).

Large-scale eruption of the intermediate-felsic igneous rocks occurred in the latest period of the ELIP event (251–253 Ma). ELIP alkaline felsic rocks such as syenite and trachyte were important sources for bauxite and Nb in the Heshan Formation (Fan et al., 2004; Wang et al., 2015). The Permian (277–252 Ma) igneous rocks that formed in response to the westward subduction between the Yangtze Plate and the Indochina Block have also been reported in many regions, mainly along the Song Ma suture zone. It is speculated that the late Permian volcanic event was widespread and produced a large amount of pyroclastic material (e.g., volcanic ash), which provided a major source for the Heshan Formation (Figure 1a; Hoa et al., 2008; Metcalfe, 2006; Halpin et al., 2016; Yu et al., 2016). In addition, abundant detrital zircons of magmatic origin related to Permian subduction have been reported from the late Paleozoic-Mesozoic sedimentary rocks on the western margin of the Yangtze block (Zhong et al., 2013; Hou et al., 2017; Ke et al., 2018; Xu et al., 2019). Therefore, Permian Paleo-Tethyan eastward-subduction-related igneous rocks might also have provided sufficient source material for the clay rocks of the Heshan Formation. Due to subsequent weathering and erosion, however, the igneous arc was not completely preserved. Island arc-type gabbro diorite and granodiorite associated with Paleo-Tethyan eastward subduction are preserved only on the eastern side of the Ailaoshan-Song Ma suture zone (Xu et al., 2020).

5.4 Sources of Nb and Li

Correlation analysis of minerals and elements show that Nb in the bauxite of the Heshan Formation is mainly hosted in anatase, which was either inherited from the parent rocks (the ELIP alkaline felsic rocks) or formed through the transformation of Ti-rich minerals in the parent rocks (Figure 6a–6b). Therefore, ELIP alkaline felsic rocks represent a common source for bauxite and Nb. During weathering and deposition, the immobile element Nb was preserved in Ti-rich minerals and gradually enriched as weathering progressed. The mechanism of enrichment of Li in clay rocks, however, is markedly different. During chemical weathering, as minerals are dissolved, active Li ions are discharged into water, which eventually flow into oceans or lakes; thus, the Li-rich clay rocks might be the product of clay minerals interacting with aquatic Li ions (Wang et al., 2006; Sun et al., 2018).

As noted above, the clay rocks of the Heshan Formation in Pingguo were formed through reactions between a Li-rich solution (pore water or groundwater) and clay minerals such as illite and pyrophyllite during diagenesis. The Heshan Formation bauxites and clay rocks formed in marine carbonate platforms; the occurrence of pisolitic and oolitic bauxite indicates a coastal environment (Table 2). The main sources of Li in pore water and groundwater during the diagenesis of Li-rich clay rock are: (1) Surface water permeation, including surface brine; (2) wall rock extraction (i.e., pore water and groundwater extracted Li from sediments and basement rocks); (3) replenishment of Li by deep hydrothermal fluids; and 4) replenishment of Li by underground brine (Tan et al., 2012; Wang et al., 2014; Sun et al., 2018). The Li concentrations in surface water (average value of 1.56 μg/L) and seawater (180 μg/L) are relatively low (You and Chan, 1996; Witherow et al., 2010), and are therefore not the main sources of the Li enrichment in pore water and groundwater. Although the Li concentration in saline lake brine is relatively high, there is abundant evidence to indicate that the Heshan Formation in Pingguo is a product of coastal deposition under warm-humid climate conditions (e.g., Hou et al., 2017; Liu et al., 2017), rather than deposition in an inland arid climate or enclosed lake basin. Therefore, saline lakes were not the main source of the Li. Although pore water-groundwater came largely from the infiltration of surface water, its interaction with wall rocks and sediments could have extracted Li and Mg to form alkaline water, which might have served as a potential source of Li. A number of studies have shown that marine sediment pore water generally has a higher Li concentration than overlying seawater, with a maximum value of 20 mg/L (e.g., Pogge von Strandmann et al., 2014; Tomascak et al., 2016).

Generally, hydrothermal fluids and underground brines (>1000 μg/L) have high Li concentrations and can serve as important sources of Li in saline lakes worldwide (Wang et al., 2006; Tan et al., 2012; Tomascak et al., 2016; He et al., 2020). The Heshan Formation, however, is composed of typical sedimentary rocks that are unrelated to hydrothermal alteration, as indicated by the results of mineralogical and geochemical studies. Deep hydrothermal fluids need not be the main source of Li for the Pingguo Li-rich clay rocks. For example, the provenance of the Carboniferous Benxi Formation bauxite in North China lies in the basement carbonates or the northern edge of the North China Plate, where there is no record of volcanic eruptions or magmatic intrusions and related hydrothermal activities (Cai et al., 2015; Wang et al., 2016). In addition, Shen et al. (1986) and Song et al. (1987) have shown that cookeite in bauxite ore-bearing rock was transformed from illite rather than by hydrothermal alteration during diagenesis. Underground brines that are rich in Ca, Na, K, Mg and Li ions may form from inland saline lakes under arid climates, and in coastal areas (Han et al., 1996). As noted previously, there are no indications of the formation of inland saline lakes and associated underground brines in the Pingguo area during the late Permian. Coastal underground brines occur in coastal sediments where they develop through evaporation, concentration, accumulation, and burial metamorphism of syngenetic seawater (Han et al., 1996). Given the depositional environment of the Li-rich clay rocks in Pingguo, this suggests that coastal underground brine was a possible source of the Li. Modern examples of abundant coastal underground brines are found in the coastal region of Shandong, Liaoning, and Tianjin in northern China (Han et al., 1996). For instance, the coastal underground brine reservoir in Laizhou Bay, Shandong, is 50–120 m thick and has a burial depth of 0–150 m, over an area of 1500 km^2; the degree of mineralization of the brine is 50–200 g/L. The brine exists in 3–4 aquifers in the coastal sandstone and clay rock layers and is characterized by its extensive distribution, high concentration, and large mineral reserves (Han et al., 1996; Su et al., 2011).

In summary, the Nb in the bauxite of the Heshan Formation in Pingguo originated mainly from the ELIP alkaline felsic rocks, and the Li in the overlying Li-rich clay rocks likely originated from groundwater or through pore-water extraction from strata and sediments, or from the direct replenishment of coastal underground brines.

6. Conclusions

In this study, mineralogical and geochemical analyses were conducted on bauxite and overlying clay rocks in the lower section of the upper Permian Heshan Formation in Pingguo, Guangxi. The preliminary conclusions are:

(1) Super-enrichment of Nb (in bauxites) and Li (in clay rocks) occurs in the Heshan Formation, and exceeds the cut-off grades for independent Nb and Li deposits. The formation is therefore highly prospective. The bauxite deposit contains a large amount of anatase, which positively correlates with the whole-rock concentrations of TiO_2 and Nb, indicating that the Nb is largely hosted in anatase. The clay rocks contain abundant cookeite, which positively correlates with Li content, indicating that cookeite is the main carrier mineral of Li.

(2) In clay rocks, cookeite coexists with clay minerals such as illite and pyrophyllite, indicating a metallogenic relationship. Combined with the characteristics of mineral assemblages, it is proposed that the cookeite formed as a result of the reaction between clay minerals and Li-Mg-rich alkaline pore water or groundwater during diagenesis. Super-enrichment of Li may be the result of extraction from wall rocks or from coastal underground brine.

(3) Provenance analysis of immobile elements and REEs indicates that the sources of the Nb-rich bauxite and the

overlying Li-rich clay rocks are distinct. The bauxite and Nb were derived largely from ELIP-related alkaline felsic rocks (e.g., A_1-types granite, rhyolite, syenite, trachyte), and the clay rocks from peraluminous or moderately fractionation felsic rocks associated with the Permian igneous arcs of Paleo-Tethys.

Acknowledgements *The authors would like to thank Prof. Yong Tang, Zhenghang Lv and Mingxing Ling for their valuable advice. We would like to express our gratitude to three anonymous reviewers and the executive editor for their review and suggestions that helped us improve the manuscript significantly. We would also like to thank senior engineers Zhiqiang Yang, Jipu Lu, Guanghui Lu, Xinyu Wang and Zhigang Liu, for their help with the geological field investigation. This study was supported by the National Key R&D Program of China (Grant No. 2017YFC0602500), the National Natural Science Foundation of China (Grant Nos. 92062107, 41703052 and 41903038), the Key Research Program of the Institute of Geology & Geophysics, CAS (Grant No. IGGCAS-201902), and the Key Research Program of the Chinese Academy of Sciences (Grant No. ZDRW-ZS-2020-4-1).*

References

Anh T V, Pang K N, Chung S L, Lin H M, Hoa T T, Anh T T, Yang H J. 2011. The Song Da magmatic suite revisited: A petrologic, geochemical and Sr-Nd isotopic study on picrites, flood basalts and silicic volcanic rocks. J Asian Earth Sci, 42: 1341–1355

Ballouard C, Poujol M, Boulvais P, Branquet Y, Tartèse R, Vigneresse J L. 2016. Nb-Ta fractionation in peraluminous granites: A marker of the magmatic-hydrothermal transition. Geology, 44: 231–234

Ballouard C, Massuyeau M, Elburg M A, Tappe S, Viljoen F, Brandenburg J T. 2020. The magmatic and magmatic-hydrothermal evolution of felsic igneous rocks as seen through Nb-Ta geochemical fractionation, with implications for the origins of rare-metal mineralizations. Earth-Sci Rev, 203: 103115

Benson T R, Coble M A, Rytuba J J, Mahood G A. 2017. Lithium enrichment in intracontinental rhyolite magmas leads to Li deposits in caldera basins. Nat Commun, 8: 270

Cai J X, Zhang K J. 2009. A new model for the Indochina and South China collision during the Late Permian to the Middle Triassic. Tectonophysics, 467: 35–43

Cai S, Wang Q, Liu X, Feng Y, Zhang Y. 2015. Petrography and detrital zircon study of late Carboniferous sequences in the southwestern North China Craton: Implications for the regional tectonic evolution and bauxite genesis. J Asian Earth Sci, 98: 421–435

Castor S B, Henry C D. 2020. Lithium-Rich Claystone in the McDermitt Caldera, Nevada, USA: Geologic, mineralogical, and geochemical characteristics and possible origin. Minerals, 10: 68

Chen J. 2019. Super-enrichment and mineralization and effective utilization of critical metals (in Chinese). Sci Tech Rev, 37: 1

Chen J Y, Yang J H. 2015. Petrogenesis of the Fogang highly fractionated I type granitoids: Constraints from Nb, Ta, Zr and Hf. Acta Petrol Sin, 31: 846–854

Dai T G, Long Y Z, Zhang Q Z, Hu B. 2007. Geological and geochemical characteristics and metallogenic mechanism of aluminium multi-metal deposits in western Guangxi (in Chinese with English abstract). J Earth Sci Environ, 29: 345−350

Dai S, Zhou Y, Zhang M, Wang X, Wang J, Song X, Jiang Y, Luo Y, Song Z, Yang Z, Ren D. 2010. A new type of Nb(Ta)-Zr(Hf)-REE-Ga polymetallic deposit in the late Permian coal-bearing strata, eastern Yunnan, southwestern China: Possible economic significance and genetic implications. Int J Coal Geol, 83: 55–63

Dai S, Li T, Seredin V V, Ward C R, Hower J C, Zhou Y, Zhang M, Song X, Song W, Zhao C. 2014. Origin of minerals and elements in the Late Permian coals, tonsteins, and host rocks of the Xinde Mine, Xuanwei, eastern Yunnan, China. Int J Coal Geol, 121: 53–78

Deng J, Wang Q, Yang S, Liu X, Zhang Q, Yang L, Yang Y. 2010. Genetic relationship between the Emeishan plume and the bauxite deposits in Western Guangxi, China: Constraints from U-Pb and Lu-Hf isotopes of the detrital zircons in bauxite ores. J Asian Earth Sci, 37: 412–424

Du S J, Wen H J, Luo C G, Gu H N, Yu W X, Li Y, Meng Y, Yang J H. 2019. Mineralogy study of Nb-rich sphene generated from the Emeishan basalts in Eastern Yunnan-Western Guizhou area, China (in Chinese with English abstract). Acta Miner Sin, 39: 253–263

Eby G N. 1992. Chemical subdivision of the A-type granitoids: Petrogenetic and tectonic implications. Geology, 20: 641–644

Ehrenberg S N, Aagaard P, Wilson M J, Fraser A R, Duthie D M L. 1993. Depth-dependent transformation of kaolinite to dickite in sandstones of the Norwegian Continental shelf. Clay Miner, 28: 325–352

Fan W, Wang Y, Peng T, Miao L, Guo F. 2004. Ar-Ar and U-Pb geochronology of Late Paleozoic basalts in western Guangxi and its constraints on the eruption age of Emeishan basalt magmatism. Chin Sci Bull, 49: 2318–2327

Fan W, Zhang C, Wang Y, Guo F, Peng T. 2008. Geochronology and geochemistry of Permian basalts in western Guangxi Province, Southwest China: Evidence for plume-lithosphere interaction. Lithos, 102: 218–236

Fang X, Galy A, Yang Y, Zhang W, Ye C, Song C. 2019. Paleogene global cooling-induced temperature feedback on chemical weathering, as recorded in the northern Tibetan Plateau. Geology, 47: 992–996

Feng J L, Gao S P, Zhang J F. 2011. Lanthanide tetrad effect in ferromanganese concretions and terra rossa overlying dolomite during weathering. Geochemistry, 71: 349–362

Förster H J, Tischendorf G, Trumbull R B, Gottesmann B. 1999. Late-Collisional Granites in the Variscan Erzgebirge, Germany. J Petrol, 40: 1613–1645

Franzini M, Leoni L, Saitta M. 1972. A simple method to evaluate the matrix effects in X-ray fluorescence analysis. X-Ray Spectrom, 1: 151–154

Fu M Y, Zhang S N, Hu W. 2012. The distribution and origin of dickite in carbonate (in Chinese with English abstract). Acta Sediment Sin, 30: 310–317

Gao Y, Yu C, Dai G G, Yang Z K. 2016. Analysis of geological characteristics and genesis of pyrophyllite ore in Taishun county white rock mining area, Zhejiang Province (in Chinese with English abstract). J Chongqing Univ Sci Tech-Nat Sci Ed, 18: 4–7

Green T H. 1995. Significance of Nb/Ta as an indicator of geochemical processes in the crust-mantle system. Chem Geol, 120: 347–359

Guangxi Bureau of Geology and Mineral Exploration and Development. 1985. Regional Geology of Guangxi. Beijing: Science Press. 212−241

Halpin J A, Tran H T, Lai C K, Meffre S, Crawford A J, Zaw K. 2016. U-Pb zircon geochronology and geochemistry from NE Vietnam: A "tectonically disputed" territory between the Indochina and South China blocks. Gondwana Res, 34: 254–273

Han Y S, Meng G L, Wang S Q. 1996. Quaternary Underground Brine in the Coastal Areas of the Northern China. Beijing: Science Press, 1–193

Hayashi K I, Fujisawa H, Holland H D, Ohmoto H. 1997. Geochemistry of ~1.9 Ga sedimentary rocks from northeastern Labrador, Canada. Geochim Cosmochim Acta, 61: 4115–4137

He H P. 2001. Study on the Interaction between Clay Minerals and Metal Ions. Beijing: Petroleum Industry Press. 1–96

He B, Xu Y G, Chung S L, Xiao L, Wang Y. 2003a. Sedimentary evidence for a rapid, kilometer-scale crustal doming prior to the eruption of the Emeishan flood basalts. Earth Planet Sci Lett, 213: 391–405

He B, Xu Y G, Xiao L, Wang K M, Sha S L. 2003b. Generation and spatial distribution of the Emeishan large igneous province: New evidence from stratigraphic records (in Chinese with English abstract). Acta Geol Sin, 77: 194–202

He B, Xu Y G, Huang X L, Luo Z Y, Shi Y R, Yang Q J, Yu S Y. 2007. Age and duration of the Emeishan flood volcanism, SW China: Geochemistry and SHRIMP zircon U-Pb dating of silicic ignimbrites, post-

volcanic Xuanwei Formation and clay tuff at the Chaotian section. Earth Planet Sci Lett, 255: 306–323
He B, Xu Y G, Zhong Y T, Guan J P. 2010. The Guadalupian-Lopingian boundary mudstones at Chaotian (SW China) are clastic rocks rather than acidic tuffs: Implication for a temporal coincidence between the end-Guadalupian mass extinction and the Emeishan volcanism. Lithos, 119: 10–19
He M Y, Luo C G, Yang H J, Kong F C, Li Y L, Deng L, Zhang X Y, Yang K Y. 2020. Sources and a proposal for comprehensive exploitation of lithium brine deposits in the Qaidam Basin on the northern Tibetan Plateau, China: Evidence from Li isotopes. Ore Geol Rev, 117: 103277
Hoa T T, Anh T T, Phuong N T, Dung P T, Anh T V, Izokh A E, Borisenko A S, Lan C Y, Chung S L, Lo C H. 2008. Permo-Triassic intermediate-felsic magmatism of the Truong Son belt, eastern margin of Indochina. C R Geosci, 340: 112–126
Hou Z Q, Gao Y F, Qu X M, Rui Z Y, Mo X X. 2004. Origin of adakitic intrusives generated during mid-Miocene east-west extension in southern Tibet. Earth Planet Sci Lett, 220: 139–155
Hou Y, Zhong Y, Xu Y, He B. 2017. The provenance of late Permian karstic bauxite deposits in SW China, constrained by the geochemistry of interbedded clastic rocks, and U-Pb-Hf-O isotopes of detrital zircons. Lithos, 278-281: 240–254
Huang H, Du Y S, Yang J H, Zhou L, Hu L S, Huang H W, Huang Z Q. 2014. Origin of Permian basalts and clastic rocks in Napo, Southwest China: Implications for the erosion and eruption of the Emeishan Large Igneous Province. Lithos, 208-209: 324–338
Huh Y, Chan L H, Edmond J M. 2001. Lithium isotopes as a probe of weathering processes: Orinoco River. Earth Planet Sci Lett, 194: 189–199
Irber W. 1999. The lanthanide tetrad effect and its correlation with K/Rb, Eu/Eu*, Sr/Eu, Y/Ho, and Zr/Hf of evolving peraluminous granite suites. Geochim Cosmochim Acta, 63: 489–508
Ke, X, Zhang, Z, Yang J, Yao H, Zhu L, He W. 2018. Radiolarian and detrital zircon in the Upper Carboniferous to Permian Bancheng Formation, Qinfang Basin, and the geological significance. J Earth Sci, 29: 594–606
Lanson B, Beaufort D, Berger G, Bauer A, Cassagnabère A, Meunier A. 2002. Authigenic kaolin and illitic minerals during burial diagenesis of sandstones: A review. Clay miner, 37: 1–22
Li X H, Li Z X, Li W X, Wang Y. 2006. Initiation of the Indosinian Orogeny in South China: Evidence for a Permian magmatic arc on Hainan Island. J Geol, 114: 341–353
Li H B, Zhang Z C, Lv L S. 2010. Geometry of the mafic dyke swarms in Emeishan large igneous province: Implications for mantle plume. Acta Petrol Sin, 26: 3143–3152
Li J M, Ding J, Yin F G, Liao C G, Chen Y, Lv T, Chen L. 2012. Regularities of distribution and geochemical characteristics of Sc in bauxite of Shenjiping mine, Southern Chongqing. Acta Sediment Sin, 30: 909–918
Ling K Y, Zhu X Q, Tang H S, Du S J, Gu J. 2018. Geology and geochemistry of the Xiaoshanba bauxite deposit, Central Guizhou Province, SW China: Implications for the behavior of trace and rare earth elements. J Geocem Explor, 190: 170–186
Ling K Y, Tang H S, Zhang Z W, Wen H J. 2020. Host minerals of Li-Ga-V-rare earth elements in Carboniferous karstic bauxites in southwest China. Ore Geol Rev, 119: 103325
Liu X, Wang Q, Feng Y, Li Z, Cai S. 2013. Genesis of the Guangou karstic bauxite deposit in western Henan, China. Ore Geol Rev, 55: 162–175
Liu X, Wang Q, Zhang Q, Yang S, Liang Y, Zhang Y, Li Y, Guan T. 2017. Genesis of the Permian karstic Pingguo bauxite deposit, western Guangxi, China. Miner Depos, 52: 1031–1048
Luo Z Y, Xu Y G, He B, Shi Y R, Huang X L. 2007. Geochronologic and petrochemical evidence for the genetic link between the Maomaogou nepheline syenites and the Emeishan large igneous province. Chin Sci Bull, 52: 949–958
MacLean W H, Bonavia F F, Sanna G. 1997. Argillite debris converted to bauxite during karst weathering: Evidence from immobile element geochemistry at the Olmedo deposit, Sardinia. Miner Depos, 32: 607–616
Mao J W, Yang Z X, Xie G Q, Yuan S D, Zhou Z H. 2019. Critical minerals: International trends and thinking (in Chinese with English abstract). Miner Depos, 38: 689–698
Masuda A, Kawakami O, Dohmoto Y, Takenaka T. 1987. Lanthanide tetrad effects in nature: Two mutually opposite types, W and M. Geochem J, 21: 119–124
McLennan S M. 1993. Weathering and global denudation. J Geol, 101: 295–303
McAulay G E, Burley S D, Johnes L H. 1993. Silicate mineral authigenesis in the Hutton and NW Hutton fields: Implications for sub-surface porosity development. Pet Geol Conf Ser, 4: 1377–1394
Metcalfe I. 2006. Palaeozoic and Mesozoic tectonic evolution and palaeogeography of East Asian crustal fragments: The Korean Peninsula in context. Gondwana Res, 9: 24–46
Mordberg L E, Stanley C J, Germann K. 2001. Mineralogy and geochemistry of trace elements in bauxites: The Devonian Schugorsk deposit, Russia. Mineral Mag, 65: 81–101
Münker C, Pfänder J A, Weyer S, Büchl A, Kleine T, Mezger K. 2003. Evolution of planetary cores and the earth-moon system from Nb/Ta systematics. Science, 301: 84–87
Nico C, Monteiro T, Graça M P F. 2016. Niobium oxides and niobates physical properties: Review and prospects. Prog Mater Sci, 80: 1–37
Nyman M W, Karlstrom K E, Kirby E, Graubard C M. 1994. Mesoproterozoic contractional orogeny in western north America: Evidence from ca. 1.4 Ga plutons. Geology, 22: 901–904
Ouahabi M, Hubert-Ferrari A, Fagel N. 2017. Lacustrine clay mineral assemblages as a proxy for land-use and climate changes over the last 4 kyr: The Amik Lake case study, Southern Turkey. Quat Int, 438: 15–29
Pédro G. 1981. Les grands traits de l'e ´volution cristallochimique des mine ´raux au cours de l'alte ´ration superficielle desroches. Rend Soc Ital Mineral Petrol, 37: 633–666
Pogge von Strandmann P A E, Porcelli D, James R H, van Calsteren P, Schaefer B, Cartwright I, Reynolds B C, Burton K W. 2014. Chemical weathering processes in the Great Artesian Basin: Evidence from lithium and silicon isotopes. Earth Planet Sci Lett, 406: 24–36
Qi L, Hu J, Gregoire D C. 2000. Determination of trace elements in granites by inductively coupled plasma mass spectrometry. Talanta, 51: 507–513
Setti M, López-Galindo A, Padoan M, Garzanti E. 2014. Clay mineralogy in southern Africa river muds. Clay miner, 49: 717–733
Shao H, Xu Y G, He B, Huang X L, Luo Z Y. 2007. Petrology and geochemistry of the late-stage acidic volcanic rocks of the Emeishan large igneous province (in Chinese with English abstract). Bull Miner Petrol Geochem, 26: 350–358
Shao J Q, Yang S Y. 2012. Does chemical index of alteration (CIA) reflect silicate weathering and monsoonal climate in the Changjiang River basin? Chin Sci Bull, 57: 1178–1187
Shellnutt J G, Zhou M F. 2007. Permian peralkaline, peraluminous and metaluminous A-type granites in the Panxi district, SW China: Their relationship to the Emeishan mantle plume. Chem Geol, 243: 286–316
Shellnutt J G, Zhou M F. 2008. Permian, rifting related fayalite syenite in the Panxi region, SW China. Lithos, 101: 54–73
Gregory Shellnutt J, Wang C Y, Zhou M F, Yang Y. 2009. Zircon Lu-Hf isotopic compositions of metaluminous and peralkaline A-type granitic plutons of the Emeishan large igneous province (SW China): Constraints on the mantle source. J Asian Earth Sci, 35: 45–55
Shellnutt J G, Jahn B M. 2010. Formation of the Late Permian Panzhihua plutonic-hypabyssal-volcanic igneous complex: Implications for the genesis of Fe-Ti oxide deposits and A-type granites of SW China. Earth Planet Sci Lett, 289: 509–519
Shellnutt J G. 2014. The Emeishan large igneous province: A synthesis. Geosci Front, 5: 369–394
Shen L P, Song Y H, Peng Z R, Guo K Z. 1986. Discovery and preliminary study of Li-chlorite in claystone from a certain location of Henan province (in Chinese with English abstract). Acta Miner Sin, 6: 86–91
Song Y H, Shen L P, Zhang N X, Peng Z R, Guo K Z. 1987. Preliminary

study on the clay minerals, rare earth elements and lithium of the clay stone (ore) from a certain location of Henan procince (in Chinese with English abstract). Sci China Ser B, 17: 204–213
Song X Y, Qi H W, Robinson P T, Zhou M F, Cao Z M, Chen L M. 2008. Melting of the subcontinental lithospheric mantle by the Emeishan mantle plume: Evidence from the basal alkaline basalts in Dongchuan, Yunnan, Southwestern China. Lithos, 100: 93–111
Su Q, Yu H J, Xu X Y, Yao J, Jiang X Y. 2011. Hydrochemical characteristics of underground brine in littoral plain south of Laizhou bay (in Chinese with English abstract). Adv Mar Sci, 29: 163–169
Sun H, Xiao Y, Gao Y, Zhang G, Casey J F, Shen Y. 2018. Rapid enhancement of chemical weathering recorded by extremely light seawater lithium isotopes at the Permian-Triassic boundary. Proc Natl Acad Sci USA, 115: 3782–3787
Sun S, McDonough W F. 1989. Chemical and isotopic systematics of oceanic basalts: Implications for mantle composition and processes. Geol Soc London Spec Publ, 42: 313–345
Sun Y, Lai X, Wignall P B, Widdowson M, Ali J R, Jiang H, Wang W, Yan C, Bond D P G, Védrine S. 2010. Dating the onset and nature of the middle Permian Emeishan large igneous province eruptions in SW China using conodont biostratigraphy and its bearing on mantle plume uplift models. Lithos, 119: 20–33
Takahashi Y, Yoshida H, Sato N, Hama K, Yusa Y, Shimizu H. 2002. W- and M-type tetrad effects in REE patterns for water-rock systems in the Tono uranium deposit, central Japan. Chem Geol, 184: 311–335
Tan H, Chen J, Rao W, Zhang W, Zhou H. 2012. Geothermal constraints on enrichment of boron and lithium in salt lakes: An example from a river-salt lake system on the northern slope of the eastern Kunlun Mountains, China. J Asian Earth Sci, 51: 21–29
Tang M, Lee C T A, Chen K, Erdman M, Costin G, Jiang H. 2019. Nb/Ta systematics in arc magma differentiation and the role of arclogites in continent formation. Nat Commun, 10: 235
Taylor, S.R., McLennan, S.M., 1985. The Continental Crust: Its Composition and Evolution. Oxford: Blackwell
Thiry M. 2000. Palaeoclimatic interpretation of clay minerals in marine deposits: An outlook from the continental origin. Earth-Sci Rev, 49: 201–221
Tomascak P B, Magna T, Dohmen R. 2016. Advances in Lithium Isotope Geochemistry. Berlin: Springer. 1–195
Vögeli N, van der Beek P, Huyghe P, Najman Y. 2017. Weathering in the Himalaya, an east-west comparison: Indications from major elements and clay mineralogy. J Geol, 125: 515–529
Vrublevskaja Z V, Delitsin I S, Zvyagin B B, Soboleva S V. 1975. Cookeite with a perfect regular structure, formed by bauxite alteration. Am Mineral, 60: 1041–1046
Wang D H, Li P G, Qu W J, Yin L J, Zhao Z, Lei Z Y, Wen S F. 2013. Discovery and preliminary study of the high tungsten and lithium contents in the Dazhuyuan bauxite deposit, Guizhou, China. Sci China Earth Sci, 56: 145–152
Wang L C, Liu C L, Cao K, Wang C L. 2014. Progress in applying non-traditional isotopes to tracing origin of brines in sedimentary basins (in Chinese with English abstract). Miner Depos, 33: 909–920
Wang Q F, Deng J, Liu X F, Zhang Q Z, Li Z M, Kang W, Cai S H, Li N. 2012a. Review on research of bauxite geology and genesis in China (in Chinese with English abstract). Geol Explor, 48: 430–448
Wang Q, Liu X, Yan C, Cai S, Li Z, Wang Y, Zhao J, Li G. 2012b. Mineralogical and geochemical studies of boron-rich bauxite ore deposits in the Songqi region, SW Henan, China. Ore Geol Rev, 48: 258–270
Wang Q, Deng J, Liu X, Zhao R, Cai S. 2016. Provenance of Late Carboniferous bauxite deposits in the North China Craton: New constraints on marginal arc construction and accretion processes. Gondwana Res, 38: 86–98
Wang Q L, Zhao Z Q, Liu C Q. 2006. New progress in lithium isotope environmental geochemistry (in Chinese with English abstract). Acta Miner Sin, 26: 196–202
Wang Q L, Chetelat B, Zhao Z Q, Ding H, Li S L, Wang B L, Li J, Liu X L. 2015. Behavior of lithium isotopes in the Changjiang River system: Sources effects and response to weathering and erosion. Geochim Cosmochim Acta, 151: 117–132
Wen H, Luo C, Du S, Yu W, Gu H, Ling K, Cui Y, Li Y, Yang J. 2020. Carbonate-hosted clay-type lithium deposit and its prospecting significance. Chin Sci Bull, 65: 53–59
Witherow R A, Lyons W B, Henderson G M. 2010. Lithium isotopic composition of the McMurdo Dry Valleys aquatic systems. Chem Geol, 275: 139–147
Wu G, Zhong D, Zhang Q, Ji J. 1999. Babu-Phu Ngu Ophiolites: A geological record of Paleotethyan Ocean bordering China and Vietnam. Gondwana Res, 2: 554–557
Wu C, Liu S, Gu L, Zhang Z, Lei R. 2011. Formation mechanism of the lanthanide tetrad effect for a topaz- and amazonite-bearing leucogranite pluton in eastern Xinjiang, NW China. J Asian Earth Sci, 42: 903–916
Wu F Y, Liu X C, Ji W Q, Wang J M, Yang L. 2017. Highly fractionated granites: Recognition and research. Sci China Earth Sci, 60: 1201–1219
Xiao L, Xu Y G, Mei H J, Zheng Y F, He B, Pirajno F. 2004. Distinct mantle sources of low-Ti and high-Ti basalts from the western Emeishan large igneous province, SW China: Implications for plume-lithosphere interaction. Earth Planet Sci Lett, 228: 525–546
Xu Y, Chung S L, Jahn B, Wu G. 2001. Petrologic and geochemical constraints on the petrogenesis of Permian-Triassic Emeishan flood basalts in southwestern China. Lithos, 58: 145–168
Xu Y G, Chung S L, Shao H, He B. 2010. Silicic magmas from the Emeishan large igneous province, Southwest China: Petrogenesis and their link with the end-Guadalupian biological crisis. Lithos, 119: 47–60
Xu J, Xia X P, Lai C, Long X, Huang C. 2019. When Did the Paleotethys Ailaoshan Ocean close: New insights from detrital zircon U-Pb age and Hf isotopes. Tectonics, 38: 1798–1823
Xu J, Xia X P, Cai K, Lai C K, Liu X J, Yang Q, Zhou M L, Ma P F, Zhang L. 2020. Remnants of a Middle Triassic island arc on western margin of South China Block: Evidence for bipolar subduction of the Paleotethyan Ailaoshan Ocean. Lithos, 360-361: 105447
Yang J, Cawood P A, Du Y. 2015. Voluminous silicic eruptions during late Permian Emeishan igneous province and link to climate cooling. Earth Planet Sci Lett, 432: 166–175
Yang S, Wang Q, Deng J, Wang Y, Kang W, Liu X, Li Z. 2019. Genesis of karst bauxite-bearing sequences in Baofeng, Henan (China), and the distribution of critical metals. Ore Geol Rev, 115: 103161
Yin K H. 2009. Mineralization and metallogenic model for bauxite in the Wuchuan-Zheng'an-Daozhen area, Northern Guizhou (in Chinese with English abstract). Acta Sediment Sin, 27: 452–457
You C F, Chan L H. 1996. Precise determination of lithium isotopic composition in low concentration natural samples. Geochim Cosmochim Acta, 60: 909–915
Yu W C, Du Y S, Zhou Q, Jin Z G, Wang X M, Qin Y J, Cui T. 2014. Provenance of bauxite beds of the Lower Permian in Wuchuan-Zheng'an-Daozhen area, northern Guizhou Province: Evidence from detrital zircon chronology (in Chinese with English abstract). J Palaeogeogr, 16: 19–29
Yu W, Algeo T J, Du Y, Zhang Q, Liang Y. 2016. Mixed volcanogenic-lithogenic sources for Permian bauxite deposits in southwestern Youjiang Basin, South China, and their metallogenic significance. Sediment Geol, 341: 276–288
Yu W, Algeo T J, Yan J, Yang J, Du Y, Huang X, Weng S. 2019. Climatic and hydrologic controls on upper Paleozoic bauxite deposits in South China. Earth-Sci Rev, 189: 159–176
Zhang Y X, Luo Y N, Yang C X. 1988. Contribution to Panzhihua-Xichang Rift, China. Beijing: Science Press. 466
Zhang Z, Mahoney J, Mao J, Wang F. 2006. Geochemistry of picritic and associated basalt flows of the western Emeishan flood basalt province, China. J Petrol, 47: 1997–2019
Zhang Z, Zheng G, Takahashi Y, Wu C, Zheng C, Yao J, Xiao C. 2016. Extreme enrichment of rare earth elements in hard clay rocks and its potential as a resource. Ore Geol Rev, 72: 191–212
Zhao X D, Ling X M, Guo H, Li J M. 2015. Geological characteristics, ore

genesis and comprehensive utilization of coexisting of Dafoyan bauxite deposit in Chongqing (in Chinese with English abstract). J Jilin Univ-Earth Sci Ed, 45: 1086–1097
Zhao Z H, Masuda A, Shabani M B. 1992. Tetrad effects of rare-earth elements in rare-metal graintes (in Chinese with English abstract). Geochimica, 3: 221–233
Zhao Z H, Xiong X L, Han X D. 1999. Discussion on formation mechanism of tetrad effects of rare-earth elements in granite—A case study of the Qianlishan and Baerzhe granites. Sci China Ser D-Earth Sci, 29: 331–338
Zhao Z H, Xiong X L, Wang Q, Qiao Y L. 2008. Some aspects on geochemistry of Nb and Ta (in Chinese with English abstract). Geochimica, 37: 304–320
Zhao L, Graham I. 2016. Origin of the alkali tonsteins from southwest China: Implications for alkaline magmatism associated with the waning stages of the Emeishan Large Igneous Province. Aust J Earth Sci, 63: 123–128
Zhao L, Dai S, Graham I T, Li X, Zhang B. 2016. New insights into the lowest Xuanwei Formation in eastern Yunnan Province, SW China: Implications for Emeishan large igneous province felsic tuff deposition and the cause of the end-Guadalupian mass extinction. Lithos, 264: 375–391
Zhao L, Dai S, Graham I T, Li X, Liu H, Song X, Hower J C, Zhou Y. 2017. Cryptic sediment-hosted critical element mineralization from eastern Yunnan Province, southwestern China: Mineralogy, geochemistry, relationship to Emeishan alkaline magmatism and possible origin. Ore Geol Rev, 80: 116–140
Zhong H, Zhu W G, Chu Z Y, He D F, Song X Y. 2007. Shrimp U-Pb zircon geochronology, geochemistry, and Nd-Sr isotopic study of contrasting granites in the Emeishan large igneous province, SW China. Chem Geol, 236: 112–133
Zhong H, Xu G W, Zhu W G, Hu R Z, He D F. 2009. Petrogenesis of the Taihe graintes in the Emeishan large igneous province and its tectonic implications (in Chinese with English abstract). Bull Miner Petrol Geochem, 28: 99–110
Zhong H, Campbell I H, Zhu W G, Allen C M, Hu R Z, Xie L W, He D F. 2011. Timing and source constraints on the relationship between mafic and felsic intrusions in the Emeishan large igneous province. Geochim Cosmochim Acta, 75: 1374–1395
Zhong Y T, He B, Xu Y G. 2013. Mineralogy and geochemistry of claystones from the Guadalupian-Lopingian boundary at Penglaitan, South China: Insights into the pre-Lopingian geological events. J Asian Earth Sci, 62: 438–462
Zhou M F, Robinson P T, Lesher C M, Keays R R, Zhang C J, Malpas J. 2005. Geochemistry, petrogenesis and metallogenesis of the Panzhihua gabbroic layered intrusion and associated Fe-Ti-V oxide deposits, Sichuan Province, SW China. J Petrol, 46: 2253–2280
Zhu J C, Li R K, Li F C, Xiong X L, Zhou F Y, Huang X L. 2001. Topaz-albite granites and rare-metal mineralization in the Limu District, Guangxi Province, southeast China. Miner Depos, 36: 393–405

(Responsible editor: Shucheng XIE)